

The kinematic identification of a thick stellar disc in M31^{1,2}

M. L. M. Collins³, S. C. Chapman³, R. A. Ibata⁴, M. J. Irwin³, R. M. Rich⁵,
A. M. N. Ferguson⁶, G. F. Lewis⁷, N. Tanvir⁸, A. Koch⁸

³*Institute of Astronomy, Madingley Rise, Cambridge, CB3 0HA, UK*

⁴*Observatoire de Strasbourg, 11, rue de l'Université, F-67000, Strasbourg, France*

⁵*Department of Physics and Astronomy, University of California, Los Angeles, CA 90095-1547*

⁶*Institute for Astronomy, University of Edinburgh, Royal Observatory, Blackford Hill, Edinburgh, UK EH9 3HJ*

⁷*Sydney Institute for Astronomy, School of Physics, A29, University of Sydney, NSW 2006, Australia*

⁸*Department of Physics & Astronomy, University of Leicester, University Road, Leicester LE1 7RH, UK*

14 November 2018

ABSTRACT

We present the first characterization of a thick disc component in the Andromeda galaxy (M31) using kinematic data from the DEIMOS multi-object spectrograph instrument on Keck II. Using 21 fields in the South West of the galaxy, we measure the lag of this component with respect to the thin disc, as well as the dispersion, metallicity and scale length of the component. We find an average lag between the two components of $\langle \Delta v \rangle = 46.0 \pm 3.9 \text{ km s}^{-1}$. The velocity dispersion of the thick disc is $\sigma_{thick} = 50.8 \pm 1.9 \text{ km s}^{-1}$, greater than the value of dispersion we determine for the thin disc, $\sigma_{thin} = 35.7 \pm 1.0 \text{ km s}^{-1}$. The thick disc is more metal poor than the thin disc, with $[\text{Fe}/\text{H}]_{spec} = -1.0 \pm 0.1$ compared to $[\text{Fe}/\text{H}]_{spec} = -0.7 \pm 0.05$ for the thin disc. We measure a radial scale length of the thin and thick discs of $h_r = 7.3 \pm 1.0 \text{ kpc}$ and $h_r = 8.0 \pm 1.2 \text{ kpc}$. From this, we infer scale heights for both discs of $1.1 \pm 0.2 \text{ kpc}$ and $2.8 \pm 0.6 \text{ kpc}$, both of which are $\sim 2\text{--}3$ times larger than those observed in the Milky Way. We estimate a mass range for the thick disc component of $2.4 \times 10^{10} M_{\odot} < M_{*,thick} < 4.1 \times 10^{10} M_{\odot}$. This value provides a useful constraint on possible formation mechanisms, as any proposed method for forming a thick disc must be able to heat (or deposit) at least this amount of material.

1 INTRODUCTION

Roughly 70% of bright galaxies observed at redshift $z = 0$ possess stellar discs (e.g. Hammer et al. 2005; Park et al. 2007; Choi et al. 2007 and Delgado-Serrano et al. (2010)), including our own Galaxy and its two largest neighbours, M31 and M33. From this, we can infer that spiral morphologies are the dominant configuration for galaxies viewed at the present epoch. Under the formalism of hierarchical structure formation, galaxies are believed to evolve into their present forms via the accretion of, and mergers with, smaller systems. The effect of this process

on the seemingly dynamically stable stellar discs we see in Milky Way (MW) type galaxies is still largely uncertain. The ability of these fragile objects to survive a “major merger” event (i.e. a merger with a system $> 1/3$ of the host’s mass) is something that is still debated. Such major mergers are thought to be cosmologically common, with $\sim 70\%$ of all galaxies with a halo mass of $M \sim 10^{12} M_{\odot}$ having experienced at least one major interaction within the past 8 Gyrs (Stewart et al. 2008; Purcell et al. 2009). Thus it has been argued that galaxies that possess thin stellar discs at $z = 0$ could not have experienced a major merger within the last 10 Gyr without the disc being destabilized (Toth & Ostriker 1992; Walker et al. 1996; Stewart et al. 2008; Purcell et al. 2009). This poses a significant challenge to our understanding of the formation of disc galaxies like the MW and M31. Recently, several authors have argued that these thin discs could survive such an event if the merging system is sufficiently gas rich (Robertson et al. 2006; Brook et al. 2007; Hopkins et al. 2009; Stewart et al. 2009; Brooks et al. 2009), although the disc would still undergo heating, resulting in a thicker disc than that observed presently in the MW. In addition to the effect of major mergers on the structure of discs, galaxies viewed at the present epoch have undergone (and

¹ The data presented herein were obtained at the W.M. Keck Observatory, which is operated as a scientific partnership among the California Institute of Technology, the University of California and the National Aeronautics and Space Administration. The Observatory was made possible by the generous financial support of the W.M. Keck Foundation.

² Based on observations obtained with MegaCam, a joint project of CFHT and CEA/DAPNIA, at the Canada-France-Hawaii Telescope (CFHT) which is operated by the National Research Council (NRC) of Canada, the Institut National des Sciences de l’Univers of the Centre National de la Recherche Scientifique of France, and the University of Hawaii.

are still undergoing) many smaller “minor” mergers which are not sufficiently massive to destroy thin stellar discs, but are thought to kinematically heat them, causing them to flare outwards and create a second, thick disc component (Quinn et al. 1993; Robin et al. 1996; Walker et al. 1996; Velazquez & White 1999; Chen et al. 2001; Sales et al. 2009; Villalobos & Helmi 2009; Purcell et al. 2010). Other physical processes are also thought to heat up and thicken the thin disc, including the accretion of a satellite on a radial orbit about its host (Abadi et al. 2003; Read et al. 2008), internal heating within the disc from massive star clusters, interactions with spiral arms, etc. (Villumsen 1985; Carlberg 1987; Sellwood & Binney 2002; Hänninen & Flynn 2002; Benson et al. 2004; Hayashi & Chiba 2006; Kazantzidis et al. 2006; Roškar et al. 2008; Schönrich & Binney 2009a; Loebman et al. 2010). Thick discs may also have formed thick, with significant star formation occurring above the mid-plane of the galaxy or with large initial velocity dispersions (Brook et al. 2004; Kroupa 2002). In recent work by Roškar et al. (2010), they suggest that in-situ formation could also occur if the stellar disc is misaligned with the hot, gaseous halo. This misalignment results in a significant warping of the outer disc, and subsequent star formation within this warp results in a low metallicity thick disc. Finally, it is also possible that a number of these mechanisms will act in conjunction. In particular, it has been suggested by a number of authors that secular growth from internal heating may be significantly enhanced by minor merger events via swing amplification (e.g. Sellwood et al. 1998; Dubinski et al. 2008), as these processes often occur simultaneously. As such, it makes little sense to treat these two scenarios as separate processes.

With so many potential mechanisms capable of producing thickened stellar discs, just how common are thick discs in spiral galaxies at the present epoch? Dalcanton & Bernstein (2002) claim that thick disc formation is a universal feature of disc formation, and as such should be observed in all spiral galaxies. Whether such discs are formed predominantly via one mechanism, or a mixture of them is still uncertain, and disentangling the various formation scenarios from one another in present data sets has proven difficult.

In the MW, the existence of a thick disc has long been known, and was first identified by Gilmore & Reid (1983). Subsequent spectroscopic studies of this component have shown it to be kinematically distinct from the thin stellar disc, with the thick disc lagging behind the thin disc by $\sim 50 \text{ km s}^{-1}$ (Carollo et al. 2010) and having a larger velocity dispersion than the thin disc. This thick component also seems to be composed of older, more metal deficient stars (e.g. Chiba & Beers 2000; Wyse et al. 2006). However the observed properties of the thick disc, such as scale height, length and velocity dispersion, tend to vary depending on the survey sample and tracer population used (Jurić et al. 2008; Ivezić et al. 2008; Carollo et al. 2010; de Jong et al. 2010). As such, the origin of the MW thick disc is still a subject of great debate in the literature. Thick discs have also been observed in a number of edge on spiral galaxies (e.g. Burstein 1979; Tsikoudi 1979; van der Kruit 1984; Shaw & Gilmore 1989; van Dokkum et al. 1994; Dalcanton & Bernstein 2002;

Elmegreen & Elmegreen 2006; Yoachim & Dalcanton 2006, 2008b,a), and spectroscopic observations of these objects also show the thick discs to be composed of older stars than their corresponding thin discs. However, as these galaxies are all located at distances greater than ~ 10 Mpc from the MW, one cannot obtain spectra for individual stars, and must instead rely on the integrated spectral properties of RGB stars. Obtaining spectra with a high enough signal-to-noise (S:N) to discern velocity dispersion profiles and reliable metallicities is also challenging, making it impossible to distinguish between the various formation mechanisms for these structures.

If thick stellar discs are universal amongst spiral galaxies, and are formed by mergers with, or accretions of, satellites, one might expect to see such a structure in M31. This neighbouring galaxy is considered to be a “typical” spiral galaxy when compared with other local external disc galaxies (Hammer et al. 2007). It is thought to have had an active merger history, and a recent panoramic photometric survey by the Pan-Andromeda Archaeological Survey collaboration (PAndAS, McConnachie et al. 2009) has shown the halo of this galaxy to be littered with tidal streams from interactions with in-falling satellites. These include the Giant Southern Stream (GSS, Ibata et al. 2001; Gilbert et al. 2009) and streams A, B, C, D and E (Ibata et al. 2007; Chapman et al. 2008; McConnachie et al. 2009). The outer disc of M31 is very perturbed (Ferguson et al. 2002; Richardson et al. 2008), suggestive of some tidal interaction. M31 is also host to 25 known dSph and 4 dE satellites, at least 2 of which (NGC 205 and M32) show evidence for significant tidal interaction (Choi et al. 2002; McConnachie et al. 2004; Geha et al. 2006; Howley et al. 2008). Therefore the possibility of numerous interactions between the disc of M31 and its satellite population seems highly likely. McConnachie et al. (2009) also present evidence for a recent interaction between M31 and its neighbouring spiral galaxy, M33, which could have significantly distorted and heated the M31 disc, giving rise to a thick disc component or substantial substructure in the outer disc. Other groups have postulated links between the formation of bulges and thick discs in spiral galaxies (Meléndez et al. 2008; Hopkins et al. 2008; Bournaud et al. 2009; Bensby et al. 2010), and as M31 is known to have a reasonably massive bulge (Saglia et al. 2010), it is an interesting candidate for hosting a thick disc. Despite its high inclination to us along the line of sight (77° , Waltherbos & Kennicutt 1988), M31 is not seen sufficiently edge-on to allow us to look for such a population using photometry. Therefore to look for evidence of a thick disc in M31, we must search for it via its kinematic signature, using spectroscopy. Given its proximity to us (785 kpc, McConnachie et al. 2005), M31 is an ideal target for spectroscopic observations as we are able to resolve and obtain reliable velocities for individual Red Giant Branch (RGB) stars, and it has an advantage over our own galaxy as we are afforded a panoramic view, whereas in the MW we are hampered along various lines of sights by confusion from the disc and the bulge.

Since 2002 our group has been conducting a systematic spectroscopic survey of M31, including the disc, halo and regions of substructure using the DEIMOS instrument mounted on the Naysmyth focus of Keck II (I05,

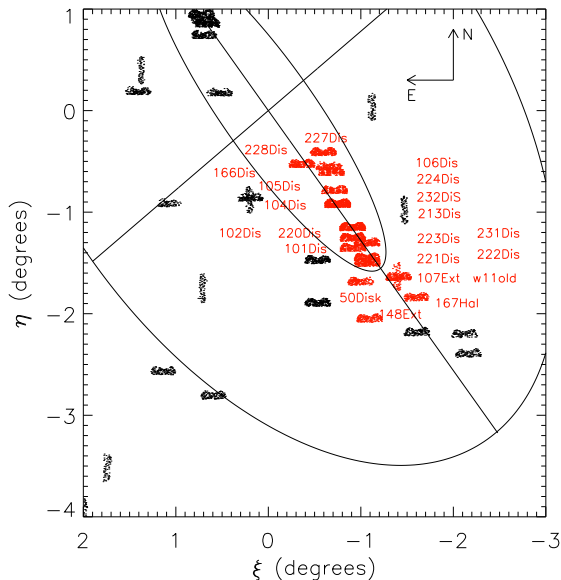


Figure 1. Map showing the location of fields within our M31 survey. Fields selected for study in this work are labelled and highlighted in red. The outer ellipse shows a segment of a 55 kpc radius ellipse flattened to $c/a=0.6$, and the major and minor axis are indicated with straight lines out to this ellipse. The inner ellipse corresponds to a disk of radius 2° , (27 kpc), with the same inclination as the main M31 disk.

Chapman et al. 2005, 2006, 2007, 2008; Collins et al. 2009, 2010). The data from this survey gives us an ideal opportunity to identify a thick disc if present. In fact, in their study of M31’s extended disc using this same data set, I05 identified a population lagging behind the thin disc which they excluded from their study that they termed a ‘thick disc-like’ population and Chapman et al. (2006) briefly examined this component as a function of radius but were unable to comment on its global properties. In this work, we discuss the results from an in depth study of this population, analysing its kinematics and chemistry, comparing them to M31’s thin and extended discs, the thin and thick discs in the MW, and those seen in other galaxies, and comment on possible formation scenarios for this component. The paper is set out as follows; in §2 we discuss the known structure of M31, §3 focuses on our spectroscopic survey of M31 and discusses field selection and analysis techniques. We present our results in §4 and discuss their implications in §5. We conclude our findings in §6.

2 THE BULGE, DISCS AND HALO OF M31

The first recorded observation of M31 was made in 964 AD in the ‘Book of constellations and fixed stars’ written by the Persian astronomer, Abd al-Rahman al-Sufi, who described it as ‘a small cloud’ in the night sky. In the centuries that have passed since, M31 has been a popular target for astronomers, and much has been learned about its structure. M31 is a spiral galaxy of SA(s)b type, with a significant

bulge, a classical thin stellar disc, a vast extended stellar disc and a metal poor halo. In this section, we outline the properties of each of these components.

First we discuss the bulge component. Numerous studies have shown that M31 possesses a classical bulge, with a Sersic index of ~ 2 and an effective radius of 1.93 kpc (Kormendy & Bender 1999; Seigar et al. 2008). It is largely supported by random motions, although recent work by Saglia et al. (2010) has found evidence for rotation in the innermost regions. Saglia et al. also find the bulge to be dominated by an old stellar population (age $\gtrsim 12$ Gyrs) of roughly solar metallicity, with a large velocity dispersion of $166\text{--}170\text{ km s}^{-1}$. This component is dominant out to about $8'$ (~ 2 kpc), at which point the disc begins to dominate the surface brightness profile of the galaxy (Saglia et al. 2010), however according to Merrett et al. (2006) the bulge can be traced out as far as 10 effective radii, equivalent to ~ 15 kpc meaning that some of our innermost disc fields may be subjected to minor contamination from this component.

Studies of the thin stellar disc of M31 have been performed by a number of authors (e.g. Waltherbos & Kennicutt 1988; Ferguson & Johnson 2001; I05; Ibata et al. 2007; McConnachie et al. 2009), and have challenged our previous notions of the structure of classical discs. With a scale length of 5.9 kpc (Waltherbos & Kennicutt 1988, corrected for assumed distance to M31 of 785 kpc, and Merrett et al. 2006), it is more extensive than that of our Galaxy, and also appears to be forming stars at a lower rate (Waltherbos & Braun 1994). And while it is a characteristic feature of the surface brightness profiles of stellar discs to steeply decline at 3–4 scale lengths (van der Kruit & Searle 1981; Pohlen et al. 2000), which corresponds to 18–24 kpc in M31, a spectroscopic study by Ibata et al. (2005) uncovered a vast, extended disc component that can be traced out to distances of ~ 40 kpc (~ 8 scale lengths) from the centre of the galaxy that has an exponential surface density profile that is very similar to the inner disc. While this structure is rather clumpy, on average it appears to follow on smoothly from the classical inner disc, although perhaps with a slightly larger scale length of 6.6 ± 0.6 kpc and with a slight lag behind circular velocities at large radii ($\langle \Delta v \rangle = 20\text{ km s}^{-1}$, I05). It is dynamically cold, with a velocity dispersion ranging from $20\text{--}40\text{ km s}^{-1}$, leading I05 to conclude that it is likely not a thickened disc. Whether this extended component is truly separate from the classical thin disc, or merely an extension of it that shows some evidence of heating and warping at larger radii where the disc is more sensitive to perturbations from mergers and interactions, is unclear. Owing to the similarity of the thin and extended discs, we will refer to them both as the ‘thin disc’ throughout this paper. Where we wish to make a distinction between the two, we shall use the terminologies ‘classical’ and ‘extended’ disc.

The presence of a smooth, pressure supported metal-poor halo in M31 eluded detection until very recently. In 2006, two groups (Chapman et al. 2006; Kalirai et al. 2006) independently identified such a component using the DEIMOS instrument on the Keck II telescope. Centred on the systemic velocity of M31, with a central velocity dispersion of 152 km s^{-1} , and showing no strong evidence of rotation, both groups found this component to be metal poor with an average metallicity of $[\text{Fe}/\text{H}] = -1.4 \pm 0.2$

(Chapman et al. 2006). Kalirai et al. (2006) were able to trace this component out as far as 165 kpc from the centre of the galaxy although there is an inevitable confusion with the halo of M33 at these large distances (Ibata et al. 2007; Koch et al. 2008; McConnachie et al. 2009).

The halo of M31 is also a known host to a number of kinematic substructures, such as the GSS, the tangential streams that cross the SE minor axis, the western shelf and a wealth of substructure in the NE of the galaxy that is thought to be linked to the GSS. In the following analysis, we will carefully consider the kinematics of all these components to ensure any thick disc sample that we define is free from contamination by any of these sources. We shall discuss this in greater detail in §3.

3 OBSERVATIONS AND FIELD SELECTION

A detailed description of the observational methodology and target selection employed in the survey is given in I05, which we briefly summarize here. Using Colour-Magnitude Diagrams (CMDs) from both the Canada France Hawaii (CFHT) and Isaac Newton (INT) telescopes (Ferguson et al. 2002; Ibata et al. 2007; McConnachie et al. 2009), we selected targets for observation by prioritising Red Giant Branch (RGB) stars in M31 with $20.5 \leq i \leq 21.2$ and colours $1.0 \leq (V - i)_0 \leq 4.0$ (priority A), then filling the remainder of the masks with stars with $I \leq 22.0$ that are unsaturated (priority B), where the V and I colours are transformed from their native g and i colours using the relations described in McConnachie et al. (2004) and Ibata et al. (2007). We used a combination of standard DEIMOS multislit mode for low density fields, such as the halo, and our own minislitlet approach which allowed us to target > 600 stars per mask in more crowded regions, such as the disc. Our observational setup covers the range of the Calcium Triplet (Ca II) lines at 8498, 8542 and 8662 Å, a prominent absorption feature that can be used both to measure radial velocities, and as a metallicity indicator. To obtain velocities, we cross-correlate all observed stars with a template Ca II spectrum. We estimate the errors on our velocities by following the procedures of Simon & Geha (2007) and Kalirai et al. (2010). First, we make an estimate of our velocity uncertainties for each observed star using a Monte Carlo method, whereby noise is randomly added to each pixel in the spectrum, assuming a Poisson distribution for the noise and the velocity is recalculated using the same cross correlation technique described above. This procedure is repeated 1000 times, and then the error is calculated to be the square root of the variance of the resulting mean velocity. We combine this error with a systematic error, ϵ , which contains information on any errors we may not have accounted for (for example, wavelength calibration error, misalignment of the mask etc.). For the fields observed with the 600 line/mm grating, we evaluate this error directly by using repeat measurements in fields 231Dis and 232Dis, a total of 332 stars. We define the normalised error, σ_N as:

$$\sigma_N = \frac{v_1 - v_2}{(\sigma_1^2 + \sigma_2^2 + 2\epsilon^2)^{1/2}} \quad (1)$$

where v_1 and v_2 , σ_1 and σ_2 are the velocities and errors of each measurement pair, and ϵ is the additional random error

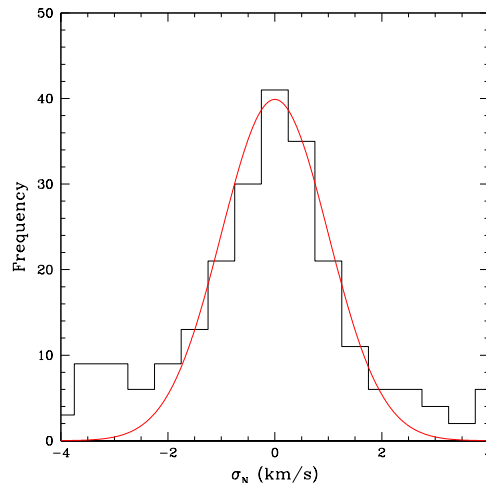


Figure 2. A histogram showing the normalized error distribution for repeat measurements of the same stars in two of our fields that were observed with the 600 lines/mm grating. The normalized error, σ_N incorporates the velocity differences between the repeat measurements (v_1 and v_2), and the Monte-Carlo uncertainties calculated for each observation (σ_1 and σ_2). In order to reproduce a unit Gaussian distribution for our uncertainties, we also include an additional error term, ϵ , which accounts for any systematic uncertainties we have not included. We find $\epsilon=5.6 \text{ km s}^{-1}$ for this setup. For fields using the 1200 lines/mm setup, we using the Simon & Geha (2007) value of $\epsilon = 2.2 \text{ km s}^{-1}$.

required in order to reproduce a unit Gaussian distribution with our data (shown in Fig. 2) This gives us a systematic error for this setup of $\epsilon = 5.6 \text{ km s}^{-1}$, slightly lower than the value of $\epsilon = 6.2 \text{ km s}^{-1}$ derived by Collins et al. (2010) for the same setup, though we note that their measurement was based on repeat observations of 47 stars, compared with our much larger data set of 332 stars. The typical uncertainties for these measurements above a threshold of S:N = 3, are $5\text{-}10 \text{ km s}^{-1}$.

The Ca II features also provide us with a method for measuring the spectroscopic metallicity of our observed sample. Following the procedure of Rutledge et al. (1997) and (Battaglia et al. 2008), we fit Gaussian functions to the three Ca II peaks to estimate their equivalent widths (EWs), and calculate $[\text{Fe}/\text{H}]$ using equation (1)

$$[Fe/H] = -2.66 + 0.42[\Sigma Ca + 0.64(V_{RGB} - V_{HB})] \quad (2)$$

where $\Sigma Ca=0.5EW_{8498}+EW_{8542}+0.6EW_{8662}$, V_{RGB} is the magnitude (or, if using a composite spectrum, the average magnitude) of the RGB star, and V_{HB} is the mean V -magnitude of the horizontal branch (HB). Using $V_{HB}-V_{RGB}$ removes any strong dependence on distance or reddening in our calculated value of $[\text{Fe}/\text{H}]$, and gives us the Ca II line strength at the level of the HB. For M31, we set this value to be 25.17 (Holland et al. 1996). We note that this assumed value is sensitive to age and metallicity effects, see Chen et al. 2009 for a discussion, however owing to the large distance of M31, small differences in this value within the disc of M31 will have a negligible effect on metallicity calculations. For individual stars, these measurements carry large errors ($\gtrsim 0.4$ dex), but the errors are significantly reduced

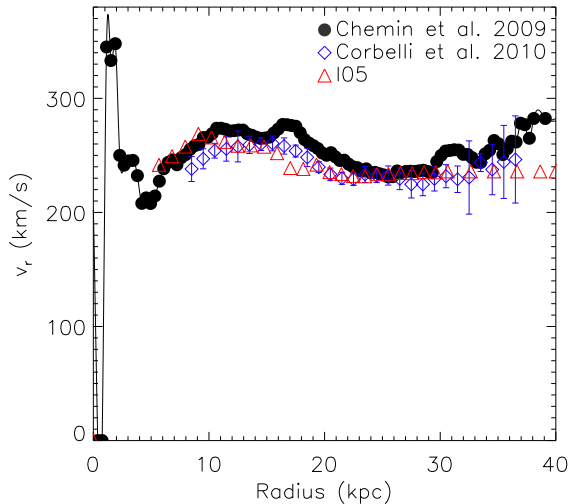


Figure 3. Here we show a number of HI rotation curves for M31. Throughout this work, we use results based on the Chemin et al. (2009) work, shown as filled black circles. We also show rotation curves from Corbelli et al. (2010) and I05, which differ slightly from the Chemin et al. 2009 curve in the outermost regions. We find that using these curves vs. the Chemin et al. (2009) results do not affect our results.

when stacking the spectra into a composite in order to measure an average metallicity for a given population.

3.1 Field selection and sample definition

In order to detect a thick disc component in M31 kinematically, we need to measure the velocities of stars within our sample relative to some model for the velocity of stars within the thin disc of the galaxy. If a thick disc is present, we should observe a population that lags behind the thin disc in terms of its rotational velocity. The component is also expected to have a larger velocity dispersion than the thin disc. This is observed in the MW, where the thick disc lags the thin by between $20\text{--}50\text{ km s}^{-1}$ (Chiba & Beers 2000; Soubiran et al. 2003) and has an average rotational velocity dispersion of $\sigma_{V_\phi} = 57\text{ km s}^{-1}$ (Carollo et al. 2010). For the purposes of this work, we shall use an updated version to the disc model of I05. In this model, we assume circular orbits for all stars about the centre of M31 and interpolate their velocities from the HI rotation curve of Chemin et al. (2009), which is shown in Fig. 3 as the solid black points. This rotation curve differs from that adopted by I05, particularly in the outermost regions. They used a compilation of CO data from Klypin et al. (2002) and HI data from Brinks & Burton (1984), which we also show in Fig. 3 as red triangles. We also show the HI rotation curve derived by Corbelli et al. (2010) from a WRST survey (Braun et al. 2009) as blue squares. Using either of these rotation curves as opposed to that of Chemin et al. leads to differences in our interpolated velocities of order a few $\text{--}20\text{ km s}^{-1}$, however there is a negligible effect on the dispersions within particular populations, and so the adoption of any of these curves would give us consistent results when analysing the global

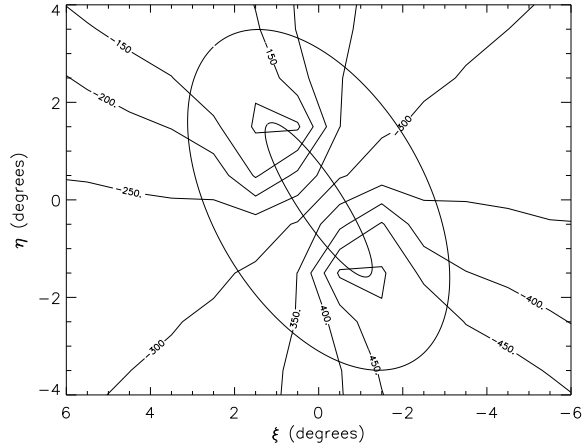


Figure 4. A contour map of the expected velocities of stars in circular orbits in the disc of M31. This was constructed using our simple model as discussed in §3.

properties of the stellar discs in this work. We assume an inclination for M31 of 77° (Walterbos & Kennicutt 1988), and adopt parameters for the thickness of the disc identical to those used in I05, with a constant thickness for the disc of 350 pc (which is roughly the thickness of the MW disc, Ivezić et al. (2008)) out to 16 kpc, at which point we assume the stellar disc begins to flare with a scale height that increases linearly with radius. We set a maximum scale height of 1.69 kpc at radius of 30.5 kpc, beyond which we assume that the disc has constant thickness. We then integrate along the line of sight through this flaring exponential disc and project the velocities of objects on circular orbits about M31 onto the line of sight. This produces an average velocity map for the disc of M31, which we display in Fig. 4.

Once our disc model has been constructed, we need to select a sample of fields from our DEIMOS survey that will provide the most reliable kinematic comparison with respect to the velocity of the disc. As the disc of M31 is not infinitesimally thin, but possesses some unknown scale height, any line of sight taken through the galaxy traverses a significant depth. Given the inclination of M31, some lines of sight will traverse larger depths than others, which could have the effect of smearing out the velocities of objects with respect to the disc model. This is illustrated in Fig. 8 of I05. They find that objects along the major axis of M31 are less susceptible to this effect than those that are located off the major axis, and therefore we limit our initial study to fields along the major axis.

A further complication in field selection arises from MW contamination. Our colour selection criteria means that we inevitably observe Galactic K dwarf stars within our sample, as these lie coincident with M31 RGB stars in the CFHT and INT CMDs. Eliminating these stars from our sample is straightforward in the South West (SW) region of M31, as the disc of Andromeda and the halo of the MW occupy distinct positions in heliocentric velocity space. Assuming the Besancon model is a good description of the foreground populations in the direction of M31, it can be shown that the Galactic population peaks at $v_{hel} = -61\text{ km s}^{-1}$, and the contribution of MW K dwarfs to our sam-

Table 1. Properties of fields analysed in this work

Field	Date observed	$\alpha_{J2000}(hh : mm : ss)$	$\delta_{J2000}(^{\circ} : ' : '')$	Grating	P.A.	Exp. time (s)	No. targets	R_{proj} (kpc)
228Dis	23/09/2006	00:40:50.56	40:43:54.0	1200 lines/mm	90°	3600s	301	9.8
227Dis	23/09/2006	00:39:37.40	40:50:42.0	1200 lines/mm	90°	3600s	312	15.6
166Dis	03/10/2005	00:39:17.89	40:42:18.0	1200 lines/mm	90°	3600s	209	15.8
106Dis	30/08/2005	00:39:10.00	40:39:00.0	1200 lines/mm	90°	3600s	257	16.1
105Dis	30/08/2005	00:39:00.00	40:28:12.0	1200 lines/mm	90°	3600s	271	16.2
224Dis	25/09/2006	00:38:50.00	40:20:30.0	1200 lines/mm	90°	3600s	265	16.6
232Dis	05/10/2006	00:38:50.00	40:20:00.0	600 lines/mm	90°	16200s	184	16.6
104Dis	30/08/2005	00:38:50.00	40:20:00.0	1200 lines/mm	90°	3600s	271	16.7
220Dis	22/09/2006	00:38:00.00	40:06:12.0	1200 lines/mm	90°	3600s	322	20.3
213Dis	22/09/2006	00:38:11.60	40:06:12.0	1200 lines/mm	90°	3600s	155	20.5
102Dis	30/08/2005	00:38:00.00	40:00:00.0	1200 lines/mm	90°	3600s	268	21.5
231Dis	05/10/2006	00:38:00.00	40:00:00.0	600 lines/mm	90°	16200s	185	21.6
223Dis	25/09/2006	00:37:12.00	39:57:00.0	1200 lines/mm	90°	3600s	304	23.2
101Dis	30/08/2005	00:38:00.00	39:54:00.0	1200 lines/mm	90°	3600s	275	23.5
222Dis	22/09/2006	00:37:12.49	39:48:06.0	1200 lines/mm	90°	3600s	298	24.9
221Dis	22/09/2006	00:37:11.97	39:45:00.0	1200 lines/mm	90°	3600s	303	25.8
50Disk	16/09/2004	00:37:35.29	39:33:55.0	1200 lines/mm	90°	3600s	216	30.1
107Ext	30/08/2005	00:35:28.00	39:36:19.1	1200 lines/mm	90°	3600s	265	31.0
w11old	30/09/2002	00:35:27.02	39:37:15.3	1200 lines/mm	90°	3600s	95	31.0
167Hal	03/10/2005	00:34:30.24	39:23:58.7	1200 lines/mm	90°	3600s	205	34.2
148Ext	04/10/2005	00:37:07.23	39:12:00.0	1200 lines/mm	90°	3600s	211	39.6

ple at $v_{hel} \leq -100 \text{ km s}^{-1}$ is very low (Robin et al. 2004, I05). Given that the average rotational velocity in the SW of M31 is less than -300 km s^{-1} (I05), we are able to cleanly separate M31 stars from MW field stars. However, in the North East (NE) of M31, the average heliocentric velocity of the M31 disc typically ranges between -100 km s^{-1} and -200 km s^{-1} , resulting in a significant overlap between Galactic and M31 populations, making it difficult to distinguish between the two. While it is possible to remove some of this contamination by examining the strength of the Sodium doublet (NaI), located at a rest wavelength of $\sim 8190 \text{ \AA}$, this is not a perfect discriminator. One can also eliminate some foreground contamination via a comparison of photometric and spectroscopic metallicities (Gilbert et al. 2006), but given the uncertainties on the individual spectroscopic [Fe/H] of our observed stars (discussed above), we still retain a significant population of contaminants within our sample. There is also contamination in the NE from M31 substructure (I05, Chapman et al. 2006; Richardson et al. 2008) which can be difficult to separate from the M31 disc in the NE. For these reasons, we limit our initial study to the SW major axis. We hope to analyse the NE population in a future paper. These criteria leave us with a sample of 21 fields along the SW major axis, highlighted in red in Fig. 1. The positions and properties of these fields can be found in Table 1. Two of these fields (231Dis and 232Dis) were observed as part of our ultra-deep M31 disc survey (Chapman et al. in prep.) and were integrated for 4.5 hours with the 600 line/mm grating, which allowed us to make more robust measurements of individual stellar metallicities than for our other fields.

To isolate a potential thick disc population in our sample of 21 fields, we must first define a statistical measure of what constitutes a lagging population with respect to the thin and extended discs. We must also ensure that our defini-

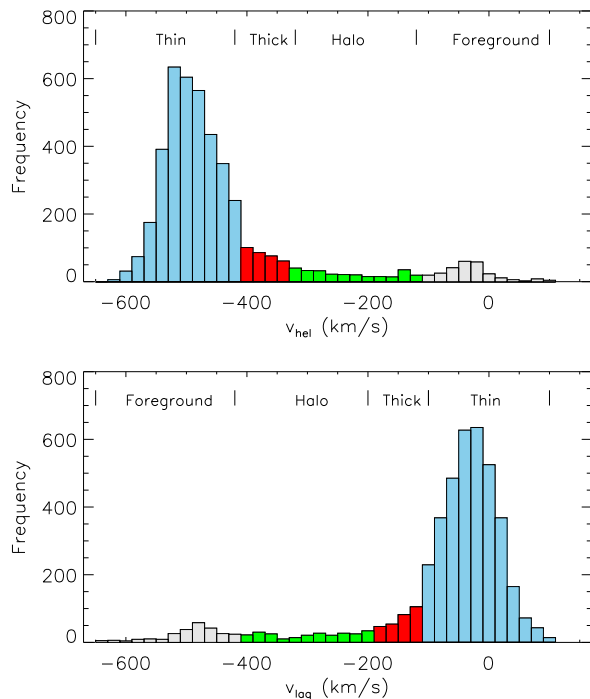


Figure 5. Histograms for both heliocentric (top) and disc lag (bottom) velocities of all stars within our sample of 21 fields. Regions expected to be inhabited by thin disc (light blue), thick disc (red), halo (green) and MW foreground (grey) are highlighted.

tion is able to distinguish between this population and that of the metal-poor M31 halo which, as it is a non-rotating component (Chapman et al. 2006; Kalirai et al. 2006), also lags behind the disc. In Fig. 5, we display two histograms,

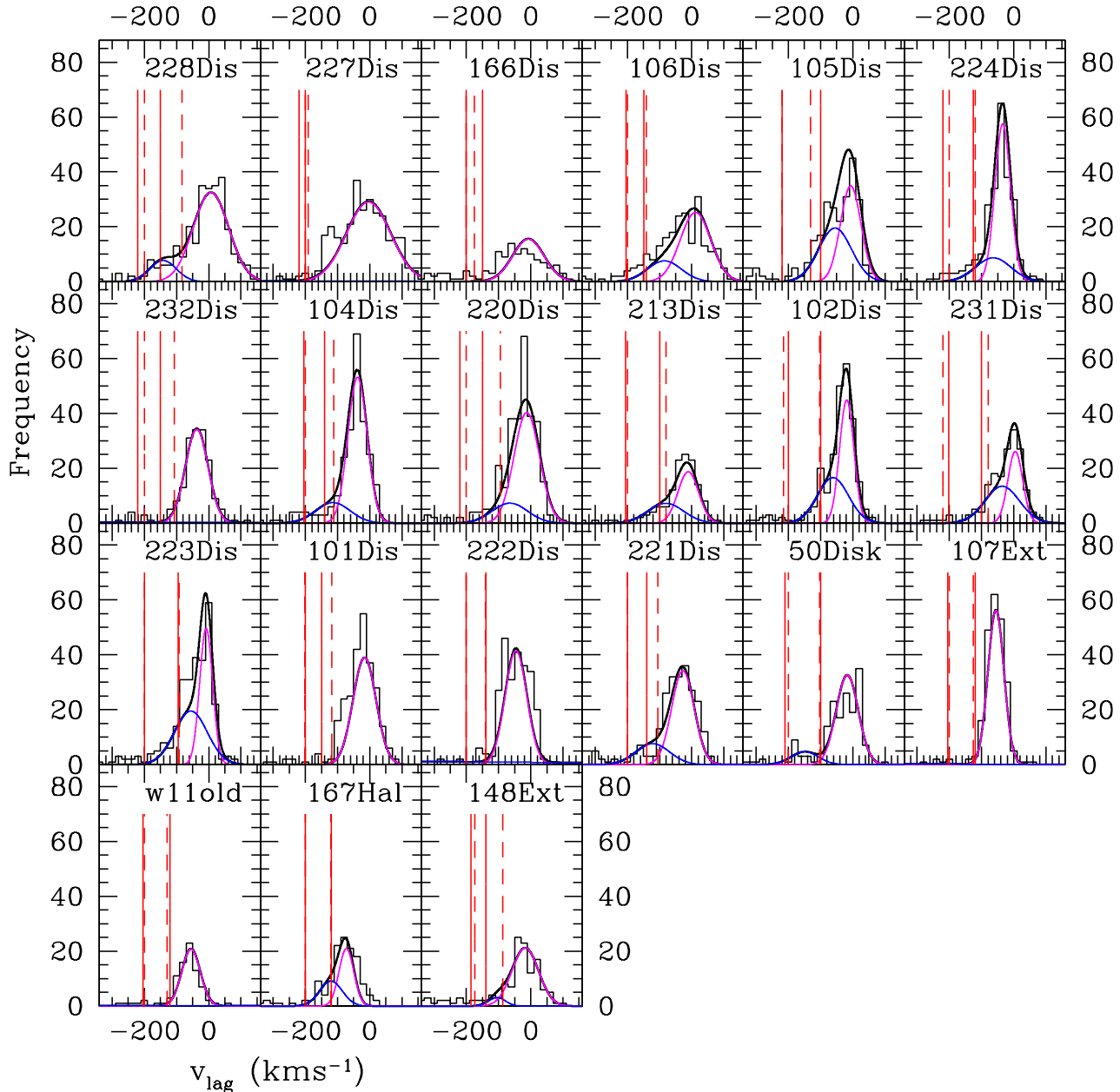


Figure 6. Our initial sample of fields, selected for their position along the South West major axis as described in the text, are shown in order of increasing (projected) radius. Gaussian fits indicating the thin and (where applicable) thick disc are shown as magenta and blue curves respectively. Our selection criteria are overlaid, with the dashed lines representing our 2σ cuts and the solid lines representing our Gaussian cuts both of which sample roughly the same region of velocity space.

one with the heliocentric velocities (v_{hel}) of the stars in our 21 fields, and one with their velocities with respect to the disc (v_{lag}) and we highlight the regions we expect each of these components to inhabit, along with where we expect to see contamination from halo K-dwarfs in the MW.

We do this using two separate methods. The first is to fit Gaussians to both a disc component, located on or around $v_{lag}=0 \text{ kms}^{-1}$, and a broad halo component centered on or around $v_{lag}=-300 \text{ kms}^{-1}$. We then define a thick disc population to encapsulate anything that lags the thin

disc by $> 2\sigma$ of the thin disc peak value and we implement a lower cut on this population by requiring the contribution from the halo would be < 1 star per velocity bin (20 kms^{-1}), thus minimizing the contamination. In fields where there is no obvious halo component to fit to, we use a Gaussian centered on -300 kms^{-1} with a dispersion of 90 kms^{-1} (Chapman et al. 2006), and normalize it with respect to the thin disc by assuming that the halo contributes $\sim 10\%$ to the total number of stars within the field (a conservative estimate, given that the stellar halo contributes $\ll 10\%$ to

the total stellar light in disc galaxies). The second method is to fit multiple component Gaussians to each of the fields. We apply a Gaussian Mixture Modelling (GMM) technique, which allows the number of Gaussians to vary freely between 1 and 7 components. To discern which model best fits the data, we apply a likelihood ratio test (LRT) to the resulting probabilities of the fits. The use of the LRT in astronomy was popularised by Cash (1979), and is often used in the literature to determine whether the properties of an observed stellar population can be well described by single vs. multiple Gaussian components (e.g. Ashman et al. 1994; Carollo et al. 2010). The LRT compares the likelihoods of nested models (in our case, a mixture of Gaussian components) to determine whether applying a model with additional parameters produces a significantly better fit than a simpler model. This is done by calculating the LRT statistic, $-2\ln(\mathcal{L}_1/\mathcal{L}_2)$, where \mathcal{L}_1 and \mathcal{L}_2 represent the likelihoods of the simple and complex model respectively, and comparing it with a χ^2 distribution with degrees of freedom equal to the difference between the number of parameters in the two models (3 in our case). For a model with additional parameters to be accepted as a statistically better fit, this ratio must be greater than 7.82 which corresponds to a P-value of < 0.05 . In general, this technique converges on fits with three components (a thin disc, a halo and a thick population) though there are a few exceptions. We shall discuss these fits in greater detail in the following section. Where this technique converges on fits that identify a lagging component that is distinct from both the thin disc and halo, we define a sample of highly probable thick disc stars by applying a standard Bayesian classification scheme to assign each star a probability of being a member of the thin disc $P(\text{thin})$, thick disc, $P(\text{thick})$, or halo, $P(\text{halo})$, population based on their velocity, and the properties of the Gaussian fits to each population on a field by field basis. We define a star as being a highly probable member of the thick disc if $P(\text{thick}) \geq 0.997$. The results of both these techniques can be seen in Fig. 6. The velocity cuts for stars selected using our 2σ technique are shown as dashed lines, and the range of velocities selected using the Bayesian classification technique are marked with solid lines. It can be seen that both techniques isolate a very similar population. In Fig. 7, we plot a CMD showing the V-I colours of the thin (blue points) and thick (magenta points) populations, and we overlay Dartmouth isochrones (Dotter et al. 2008) of $[\alpha/\text{Fe}] = +0.2$ and an age of 8 Gyrs (in line with the estimated range of ages for the thin disc of 4–8 Gyrs, Brown et al. 2006) with metallicities ranging from $[\text{Fe}/\text{H}] = -0.4$ to $[\text{Fe}/\text{H}] = -1.5$. Both thin and thick populations inhabit roughly the same region in this CMD, which we shall discuss in more detail in §4.3.

Finally, we note that in both selection methods, we expect some cross contamination between the thin and thick disc components, as the two populations significantly overlap. However, we assume this contamination will be lower in our cuts based on the Gaussian fits, as these are more conservative. Therefore, we use these cuts predominantly in this paper when referring to clean thin and thick disc samples. We have also assumed both components have symmetric, Gaussian distributions in velocity, which may not be the case, and this could cause further contamination if the populations are skewed. We also expect some contamination from the halo, however, given that the disc is the dominant

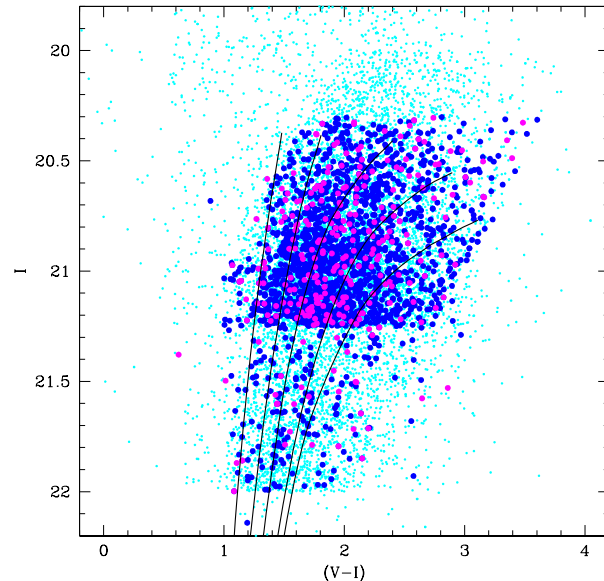


Figure 7. CMD for our thin (blue points) and thick (magenta points) populations in standard Landolt V and I colours. Dartmouth isochrones with $[\alpha/\text{Fe}] = +0.2$ and an age of 8 Gyrs are overlaid with metallicities from left to right of $[\text{Fe}/\text{H}] = -1.5, -1.0, -0.5, -0.4$. The colours of the remaining stars in our DEIMOS survey are also plotted in light blue.

population in all our fields, we expect this contamination to be negligible in comparison to the cross contamination between the discs.

3.2 Testing the statistical significance of our sample

Before we analyse our sample, we test the significance of our thick population to ensure it is not merely consistent with noise above a thin disc population plus smooth halo component. To do this, we fit a single Gaussian to the disc and halo components, as described above, then calculate the deviation of the data from the fit for all velocities greater than the peak disc velocity (i.e. the right hand side of the disc fit), normalizing it to the expected contribution from the Gaussian in this region. We then define the noise to be 1.5 times the median absolute deviation of this sample. We repeat this exercise for all velocities less than the thin disc peak and greater than -200 km s^{-1} in the lag frame, in this case comparing to the expected contribution from both thin disc and halo fits. This allows us to work out the significance of our thick disc population, σ_{conf} . In all cases where the GMM identified a thick disc component, we find that our excess above the thin disc plus halo model has a significance of $> 3\sigma$ (see table 2). For the fields where the GMM converged on a 2 Gaussian fit (232Dis, 222Dis, 107Ext and w11old), we find $\sigma_{conf} < 3\sigma$. We also identify an additional 3 fields (101Dis, 166Dis and 227Dis), where $\sigma_{conf} < 3\sigma$. Two of these fields are located at radii of $\sim 15 \text{ kpc}$, where there may be residual contamination from the bulge component. This may also explain the large dispersions (of order 50 km s^{-1}) seen in our innermost fields. Excluding these, we

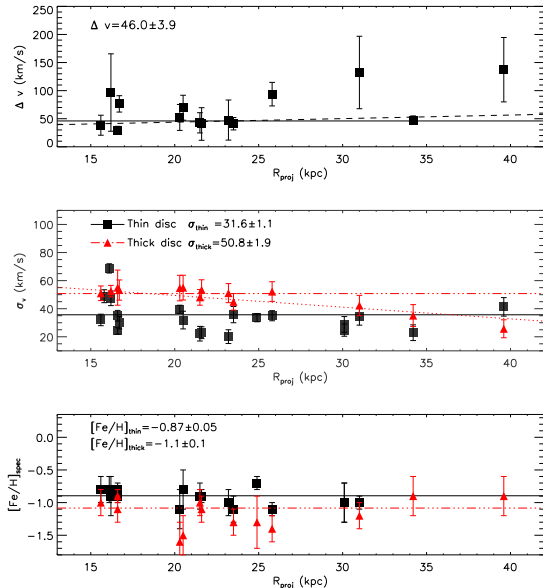


Figure 8. Top panel: The difference in velocity, Δv , between the thin disc and thick component as a function of projected radius. This lag appears to be approximately constant as a function of radius, with an average lag of $46.0 \pm 3.9 \text{ km s}^{-1}$. There appears to be a slight increase in lag in the outermost part, however this is largely driven by fields that lie off the major axis of M31, and therefore the velocities are less reliable. **Middle panel:** Dispersion, σ_v , of both thin (black squares, solid line) and thick (red triangles, dot-dashed line) components are plotted as a function of projected radius. The thin disc appears to maintain a constant dispersion of $\sigma_{thin} = 31.7 \pm 1.0 \text{ km s}^{-1}$, however the thick component appears to decrease somewhat at larger radii. **Bottom panel:** Average spectroscopic metallicity of thin and thick components as a function of projected radius. Neither component evolves with radius.

are left with 14 of our 21 (2/3) fields where we confidently detect a thick component. We shall focus on these fields in the remainder of our analysis, but we shall discuss the significance of the non-detections in §5.

4 RESULTS

4.1 Kinematic and structural properties of the thin and thick discs

In this section we present measurements for the kinematic and structural properties of the thin and thick discs. Properties of individual fields can be found in Table 2, while the average properties for both components can be found in Table 3.

4.1.1 Velocity lag and dispersion profiles

In this first section, we initially address the thin and extended discs of M31. In I05, the extended disc was identified as a stellar disc that, while appearing in many respects to be similar to the classical thin disc, was a separate entity that was clumpy in terms of its structure, and lagged behind the classical disc in terms of its kinematics. As we are

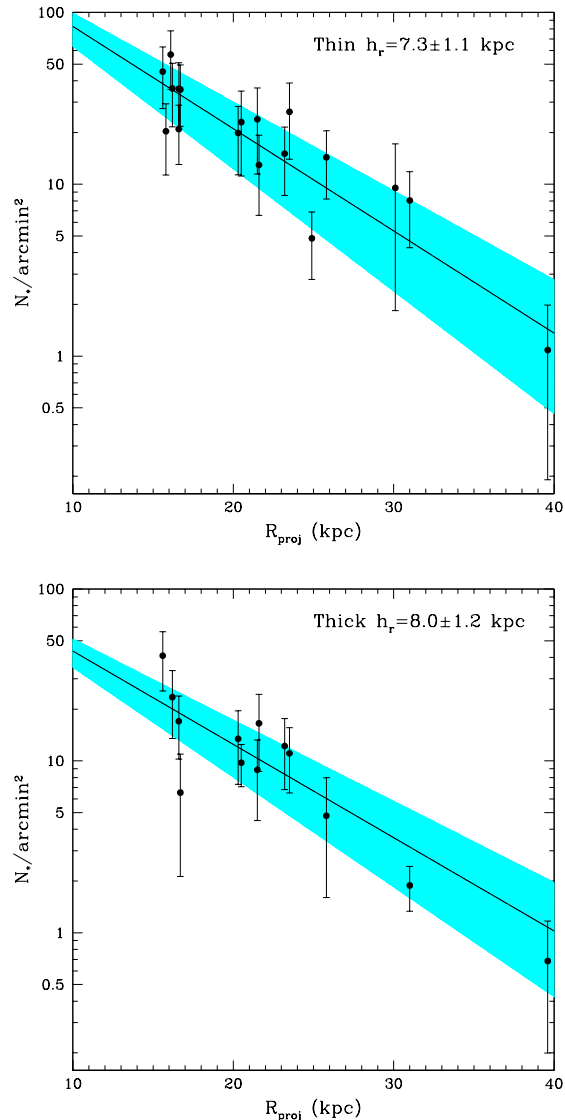


Figure 9. Top panel: Plot of the density of stars (N_*/arcmin^2) in the thin disc against R_{proj} . The densities are calculated by first separating our sample by their target prioritisation (A or B, see §3), then counting all stars with $v_{thin} > v_{lag} > v_{thin} + 2\sigma_{thin}$ and multiplying these values by 2 (i.e. assuming the distributions are symmetric) for both prioritisations. We then calculate $\rho_* = n_s n_t / n_o - n_b$, and combine these results from priority A and B. Fitting an exponential profile to these points we deduce $h_r = 7.3 \pm 1.1 \text{ kpc}$. Solid line represents the best fit to the data from a weighted-least-squares routine, and the shaded region indicates the 1σ errors from the fit. **Bottom panel:** As above, for the thick disc. Here we count all stars with $v_{thick} - 2\sigma_{thick} > v_{lag} > v_{thick}$ and multiply by two again. Fitting an exponential profile to these points we deduce $h_r = 8.0 \pm 1.2 \text{ kpc}$.

limiting our study to one slice down the major axis of M31, we do not attempt to comment on the global ‘clumpiness’ of this extended disc, but we return to the issue of the velocity lag and distinction from the thin stellar disc. As we have analysed the disc frame velocities for all our fields using a rotation curve that differs from the one used in I05, it is useful for us to determine whether the increasing lag

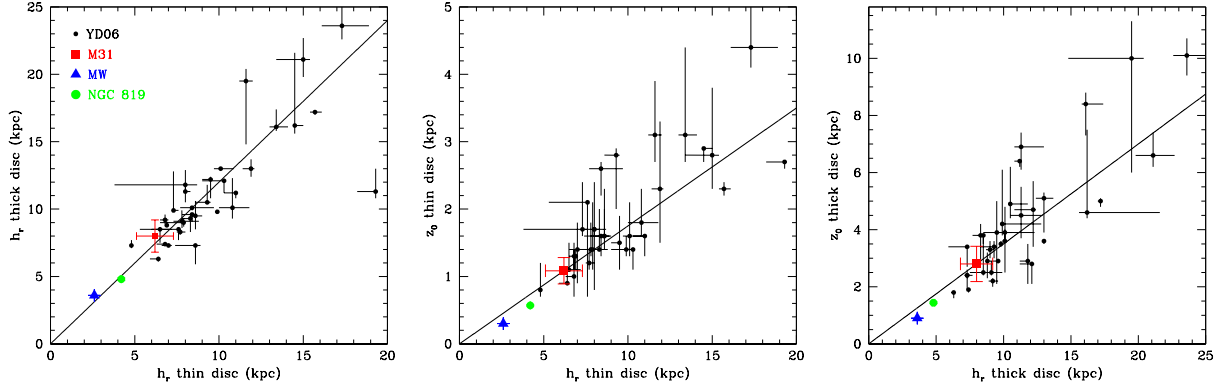


Figure 10. Here we compare the scale lengths of the thin and thick discs in M31 to those of other galaxies with observed thick discs in order to infer their scale heights. **Left panel:** Here we plot thin disc scale lengths against thick disc scale lengths for 34 external galaxies (YD06) as black points, and overplot the same measurements for the MW (blue triangle). We fit a linear relation to these points with a gradient of 1.3. We plot our result for M31 as a red square, and it is in excellent agreement with this relation. **Centre panel:** Here we plot scale height, z_0 , against scale height for the thin disc of the YD06 sample plus the MW and derive a best-fit linear function with a gradient of 0.17. From this, we can estimate a scale height for the M31 thin disc of 1.1 ± 0.2 kpc, which we overplot on the relation as a red square. **Right panel:** We now plot the same, but for the thick disc and find a best fit gradient of 0.35, and therefore infer a scale height for the thick disc in M31 of 2.8 ± 0.6 kpc, which is overplotted as a red square.

with respect to the classical thin disc is seen here also. In I05, they split their sample of 21 fields into an inner (with $R_{proj} < 20$ kpc) and outer (with $20 < R_{proj} < 30$ kpc) sample to determine the average properties of the disc and extended disc. For their inner (classical) disc sample, they calculated an average velocity for the disc in the disc lag frame of $v_{lag} = -17.0 \text{ km s}^{-1}$ and a dispersion of $\sigma_v = 50.0 \text{ km s}^{-1}$. In the outer (extended) sample they calculated an average velocity of $v_{lag} = -16.0 \text{ km s}^{-1}$ and a dispersion of $\sigma_v = 51.0 \text{ km s}^{-1}$. If we perform the same analysis for our study, we find an average lag of $v_{lag} = -14.8 \text{ km s}^{-1}$ for our inner fields and $v_{lag} = -25.5 \text{ km s}^{-1}$ for our outer fields. However, we note that this value is calculated with the inclusion of fields 107Ext, w1old and 167Hal, which have very large lags of $v_{lag} < -55 \text{ km s}^{-1}$ compared with the other fields. We note that these fields are located slightly off the semi major axis (see Fig. 1) where our interpolated disc-frame velocities are subject to larger uncertainties. If we exclude these fields, we find an average lag of $v_{lag} = -14.9 \text{ km s}^{-1}$, very similar to our inner sample. We therefore conclude that there is a negligible difference in the lags of the classical and extended disc behind circular velocities. For these samples we also calculate average dispersions of $\sigma_v = 42.7 \text{ km s}^{-1}$ and $\sigma_v = 30.0 \text{ km s}^{-1}$, implying that the extended disc has a lower dispersion than the classical disc. However, in our inner sample, we are more likely to see residual contamination from the bulge and we also have a large proportion of fields for which we could not cleanly isolate the thick disc ($\sim 40\%$ cf. $\sim 20\%$ in the outer sample). These factors may cause us to overestimate the dispersion of the disc in these regions. From these results, we therefore find no concrete reason to assume that the extended disc is a separate component from the classical disc and we treat these two components as one thin stellar disc in the remainder of our analysis.

By using the information from our Gaussian fits to the thin and thick components, we can comment on their global kinematic properties, and discuss any variation of

these properties with radius. In Table 2 we show the peak velocities and velocity dispersions of both thin and thick (where applicable) components in each field, with associated errors from the GMM fits. Where both thin and thick components are detected, we compute the lag between the two components, $\Delta v = v_{thin} - v_{thick}$, and plot this lag as a function of radius in Fig. 8. The 14 fields for which a thick disc component is reliably detected cover a range of radii from 15.2 to 39.6 kpc. In the top panel of Fig. 8, we can see that the lag between the two components does not appear to increase with distance from the centre of M31, and shows an average lag of $\langle \Delta v \rangle = 46.0 \text{ km s}^{-1}$.

We also plot the dependence of velocity dispersion, σ_{thin} and σ_{thick} , for both components with radius in the middle panel of Fig. 8. For the thin disc, we fit both a constant relation and a single power law to the data. The linear power law suggests a decrease in dispersion with radius, with a gradient of $-0.87 \text{ km s}^{-1} \text{ kpc}^{-1}$, however this fit is not statistically better than a constant fit, with an average dispersion of $\sigma_{thin} = 31.6 \pm 1.1 \text{ km s}^{-1}$ (reduced χ^2 of 5.6 vs. 5.2). We do the same for our thick disc results, and we find that a linearly decreasing profile where $\sigma_{thick} = -0.8(\pm 0.2)R_{proj} + 66.1(\pm 5.8)$ has a marginally better fit to the data than a fit with no evolution, however the difference is negligible (reduced χ^2 of 1.2 vs. 1.4), and deemed insignificant in a χ^2 significance test. Even if we were to accept this fit as preferred, we note that the two outermost fields situated at 34.2 and 39.6 kpc, are perhaps the driving force in the decreasing dispersion seen in our thick disc component. As these field are the furthest out in our survey, they also suffers from the greatest chance of halo contamination in our sample, and therefore could be unreliable. If we exclude these final points from the fit, we find that σ_{thick} is best fit with no evolution as a function of radius, with an average dispersion of $50.8 \pm 1.9 \text{ km s}^{-1}$. We therefore conclude that our data cannot tell us anything reliable about the dependence of these kinematic properties

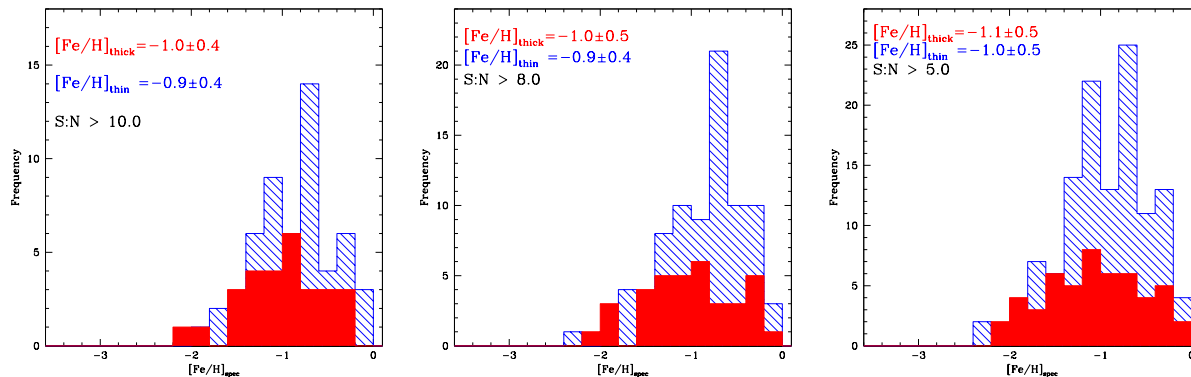


Figure 11. Here we display the spectroscopic MDF for all stars in our thin and thick components (shown as blue hatched and red solid histograms respectively) In the left panel, we show the MDF using all stars for which metallicities can be reliably measured (i.e. $S:N \geq 10 \text{ \AA}^{-1}$), and the middle and right panels apply lower quality cuts ($S:N \geq 8 \text{ \AA}^{-1}$ and $S:N \geq 5 \text{ \AA}^{-1}$). For our lower $S:N$ cuts, we note that the median $[\text{Fe}/\text{H}]$ values for both populations remain similar, and the dispersions (inter-quartile range) begin to increase, losing some of the detail of the shape of the MDF. In all cases the median $[\text{Fe}/\text{H}]$ of the thick disc is more metal poor than the thin by ~ 0.1 dex.

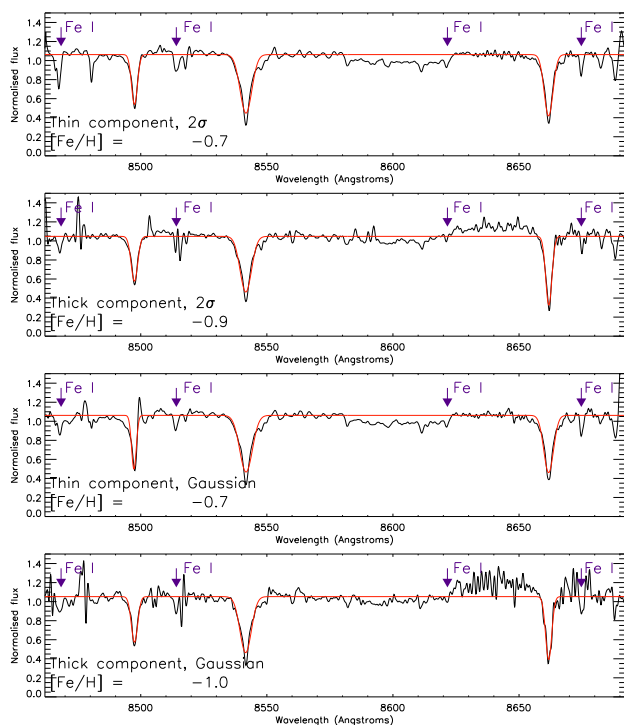


Figure 12. Composite spectra of both the thin disc and thick component, using both 2σ (top panel) and Gaussian (lower panel) cuts to isolate the thick component. The composite spectra are constructed from stars within the selection regions that possess a $S:N \geq 3.0 \text{ \AA}^{-1}$. We find that the average metallicity for the thin component is more metal rich than the thick by 0.2–0.3 dex. These results are consistent with composites formed from spectra with $S:N \leq 3 \text{ \AA}^{-1}$ and with our field-by-field metallicity estimates (Fig. 8). We also show the locations of a number of Fe I lines present in these spectra.

with radius, and allow us to merely calculate the average kinematics of both components.

4.1.2 Scale length of the thin and thick disc

To determine the scale lengths of our two disc components, we need to calculate the number density of thin and thick disc stars within our DEIMOS field of view. There are 2 complications we must consider before we proceed. Firstly, the two components are not completely distinct from one another, and in all fields, we observe some overlap. Secondly, owing to our selection criteria (discussed in § 3), we prioritise stars of certain colours and magnitudes above others, and this must be considered when calculating densities on a field-by-field basis.

We determine the number of stars associated with the extended thin disc, n_s , in each of our fields by integrating the Gaussian we have fit to this component. To determine the density of stars contained in the thin disc, we multiply n_s by the total number of available target stars within our DEIMOS field that fall within our selection criteria, n_t , and divide this by the total number of stars that were observed with our DEIMOS mask, n_o . We then subtract the density of background stars n_b , which is computed from a number of fields on the edge of our survey region; i.e. $\rho_* = n_s n_t / n_o - n_b$. To account for our prioritised selection technique, we perform this calculation separately for our priority A and priority B stars, then combine these measurements. We repeat this calculation for the thick disc. We plot the results in Fig. 9, where we apply a weighted least-squares exponential fit to our data points, and determine $h_r = 7.3 \pm 1.1$ kpc for the thin disc and $h_r = 8.0 \pm 1.2$ kpc for the thick. Comparing this to previous calculations for the scale length of the thin and extended discs, we find that the extended disc has a larger scale length than the exponential thin disc, (5.1 ± 0.1 kpc, I05). The value of 7.3 kpc that we derive is slightly higher than that derived in I05 of 6.6 ± 0.4 kpc, and with much larger error bars but the two are consistent within their 1σ uncertainties. The difference between the

two values can be attributed to two factors. Firstly, in I05, they included fields from the NE of the galaxy, plus fields located away from the major axis, where we have sampled fields solely from the SW major axis. Secondly, in I05 they did not fully address any biases that may have been introduced by our two-tiered prioritisation system. Finally, we note that the thick disc appears to be more radially extended than either the thin or extended disc, although it is consistent with the scale length of the extended disc within its 1σ -errors.

In previous work Yoachim & Dalcanton (2006) (hereafter YD06) measured the scale lengths of 34 edge-on disc galaxies using a photometric fitting technique, and found that the scale lengths of the thick discs were larger than those of the thin discs by a factor of ~ 1.3 . We plot their results in the left panel of Fig. 10, and overlay a linear relation with a gradient of 1.3. We add to this our results for M31, using an average value for the thin disc from the range of scale lengths derived for the thin and extended discs (5.1–7.3 kpc) of 6.3 kpc, and our calculated value of 8.0 kpc. We also overplot the result for the MW (using Jurić et al. 2008 values of 2.6 and 3.6 kpc for thin and thick discs respectively), and note that M31 sits in excellent agreement with this relation.

4.1.3 Inferring the scale heights of the thin and thick discs

Owing to the inclination of M31, we are unable to measure the height of either the thin or thick disc components directly. No photometric excess above a typical bulge or extended disc profile is observed when performing minor axis star counts (Irwin et al. 2005), suggesting that these components dominates the surface profile out to large radii. In order to infer probable scale heights for both components, we make use of the properties of the 34 edge-on galaxies measured by YD06. As the scale lengths and heights of both thin and thick discs in each of these galaxies were derived, it is possible for us to search for a relation between the scale length, h_r , and scale height, z_0 of each component. In the central panel of Fig. 10, we plot h_r vs. z_0 for the YD06 sample as well as for the MW (Ivezić et al. 2008), and fit it with a linear relation, on which we force an intercept of (0,0). We find that the data are well fit with a gradient for this relation of 0.18 ± 0.04 , though there is significant scatter beyond ~ 9 kpc. From this, we deduce $z_0 = 1.1 \pm 0.2$ kpc for the M31 extended disc (using $h_r = 7.3$ kpc). We repeat this for the thick disc (shown in the right panel of Fig. 10) and find that these values are well fit with a linear relation of gradient 0.35 ± 0.06 , giving us $z_0 = 2.8 \pm 0.6$ kpc for the M31 thick disc. If these values are correct, then not only are the discs of M31 more radially extended than those of the MW by a factor of $\sim 2 - 3$, they are also significantly thicker.

4.1.4 Contrast of the thin and thick discs

In the previous sections, we have derived the density in each field of both our components as a means to determine the scale lengths. We now use these densities to work out how much of the total (disc related) stellar population is contained within either component. There are several caveats to such a comparison that should be mentioned. Firstly, our

sampling of the field is likely to have an effect on our field-to-field estimates of the stellar density (which we discuss further in § 5). Secondly, as the disc is not observed edge-on, we are measuring a 2D projection of the densities which is difficult to interpret. We also note that the measurement errors associated with the densities of each field (shown in table 4) are significant (of order $\sim 50\%$).

With this in mind, we find that, on average, the thick disc component accounts for 35% of the total stellar density, with an inter-quartile range of $\pm 10\%$. In the Milky Way, we know that the thick disc contributes to $\sim 10\%$ of the stellar density in the solar neighbourhood, and accounts for $\sim 1/3$ of the *total* disc mass (Jurić et al. 2008; Schönrich & Binney 2009a), comparable to what we derive here.

From our calculated contrasts and individual density profiles for the thin and thick discs, we can estimate the mass contained within the thick disc component using values for the mass of the thin disc from the literature. From our analysis above, we have determined that the thick disc contributes $35 \pm 10\%$ of the *total* stellar density, meaning the thick:thin disc density ratio is of order $55 \pm 15\%$. We can also estimate this fraction by integrating our stellar density profiles (Fig. 9) over the limits of our data, and from this we calculate a thick:thin disc density ratio of $\sim 65\%$, which is in good agreement with our contrast estimate. If we assume that both discs are composed of similar stellar populations, we can set the mass ratio between the disc to be equivalent to the density ratio. In Yin et al. (2009), they quote a total mass for the thin stellar disc of $M_{*,thin} = 5.9 \times 10^{10} M_\odot$, calculated from the mass models of Widrow et al. (2003) and Geehan et al. (2006). From this we estimate that the total mass of the M31 thick disc lies in the range $2.4 \times 10^{10} M_\odot < M_{*,thick} < 4.1 \times 10^{10} M_\odot$. As we are unable to determine the full radial and underlying luminosity profile for the thick disc, these values are obviously prone to large errors introduced by our simplifying assumptions, and the mass of the thick disc may be lower than our quoted range. For example, if we just compare the number of stars we detect in the thin disc throughout our entire sample with the number we detect in the thick disc by integrating the fitted Gaussians in Fig. 6 we find a thick:thin disc ratio of 20%. If we assume this value for the ratio of the masses between the components, our lower limit on the thick disc is reduced to $M_{*,thin} = 1.2 \times 10^{10} M_\odot$. A future study of the thick disc which includes fields from the entirety of our survey will help us to better constrain both the radial profile and mass of this component.

4.2 Spectroscopic metallicities

In this section we present the spectroscopic values of [Fe/H], both for individual stars, and for the composite spectrum of each component. Measuring individual metallicities from the Ca II triplet for the stars in our survey, with S:N typically between $5 - 15 \text{ \AA}^{-1}$, is quite problematic. In Battaglia et al. (2008), they show that the ‘best case’ errors in measuring the equivalent widths of the Ca II lines, ΔEW , scale with S:N as:

$$\Delta EW = \frac{\sqrt{1.5 \times FWHM}}{S : N} \quad (3)$$

Table 2. Kinematic properties of thin and thick disc components

Field	$v_{thin,lag}$ (km s ⁻¹)	σ_{thin} (km s ⁻¹)	$v_{thick,lag}$ (km s ⁻¹)	σ_{thick} (km s ⁻¹)	σ_{conf}	[Fe/H] _{thin}	[Fe/H] _{thick}
228Dis	6.8±5.0	55.2±3.2	-141.9±7.5	41.2±11.8	37.0	-0.8±0.1	-1.0±0.1
227Dis	-3.7±10.8	68.7±3.3	N/A	N/A	2.8	-0.7±0.2	N/A
166Dis	-7.5±6.9	48.9±4.6	N/A	N/A	0.5	-0.8±0.2	N/A
106Dis	11.6±8.2	47.4±5.2	-85.0±8.2	52.5±4.1	3.5	-0.9±0.3	-1.0±0.3
105Dis	-16.4±7.2	32.0±4.1	-54.8±8.7	51.0±5.2	4.0	-0.7±0.2	-1.0±0.2
224Dis	-34.4±6.2	24.3±2.5	-63.8±10.2	55.0±12.5	5.1	-0.9±0.1	-1.1±0.2
232DiS	-37.2±3.0	35.0±3.8	N/A	N/A	2.0	-0.8±0.1	N/A
104Dis	-37.9±6.5	30.0±4.4	-114.3±9.5	53.3±7.2	9.0	-0.7±0.2	-0.9±0.1
220Dis	-12.5±5.0	39.6±2.9	-64.8±12.1	54.7±10.9	26.7	-1.1±0.3	-1.6±0.3
213Dis	-10.9±3.2	31.9±6.3	-80.5±10.0	55.0±8.8	39.2	-0.8±0.3	-1.5±0.3
102Dis	-18.8±7.1	22.2±5.2	-61.5±11.6	48.1±5.6	47.1	-0.9±0.2	-1.0±0.2
231Dis	4.7±15.2	22.9±4.2	-35.9±7.8	53.4±7.2	43.4	-0.9±0.1	-1.1±0.2
223Dis	-8.1±5.9	20.1±4.9	-55.7±9.9	51.1±6.8	14.7	-0.7±0.2	-1.0±0.3
101Dis	-16.2±3.9	35.8±5.8	-57.3±8.6	44.9±6.2	3.1	-1.1±0.2	-1.3±0.3
222Dis	-25.9±4.8	33.6±2.9	N/A	N/A	0.8	-0.7±0.1	N/A
221Dis	-27.5±5.5	35.0±3.6	-121.2±7.4	52.2±6.3	27.1	-1.1±0.2	-1.4±0.2
50Disk	-16.9±8.1	34.2±5.9	-149.2±13.2	42.3±7.2	12.6	-1.0±0.2	-1.2±0.2
107Ext	-55.2±6.9	24.8±4.4	N/A	N/A	2.4	-1.0±0.3	N/A
w1old	-55.1±10.2	28.8±5.6	N/A	N/A	1.4	-1.0±0.3	N/A
167Hal	-72.6±8.3	22.9±5.4	-120.3±12.2	35.1±7.8	23.5	-0.9±0.3	-1.0±0.3
148Ext	-17.2±7.0	41.3±6.6	-154.5±11.0	25.7±5.1	28.2	-0.9±0.3	-1.0±0.2

Table 3. Average properties of thin and thick disc components derived in this work

Component	σ_v (km s ⁻¹)	h_r (kpc)	z_0 (kpc)	[Fe/H] _{spec}
Thin disc	35.7±1.0	7.3±1.1	1.1±0.2	-0.7±0.05
Thick disc	50.8±1.9	8.0±1.2	2.8±0.6	-1.0±0.1

Table 4. Field by field densities of thin and thick disc stars

Field	ρ_{*thin} (* / arcmin)	ρ_{*thick} (* / arcmin)
228Dis	57.6±22.3	N/A
227Dis	56.9±22.3	N/A
166Dis	20.4±9.4	N/A
106Dis	36.2±15.3	23.6±10.5
105Dis	45.3±18.6	41.0±16.3
224Dis	20.1±8.4	17.1 ±7.1
232DiS	35.9±15.7	N/A
104Dis	35.7±14.6	6.6±4.5
220Dis	19.9±8.9	13.5±6.4
213Dis	23.0±12.2	9.8±3.0
102Dis	24.0±12.8	8.9±4.5
231Dis	13.0±6.6	16.6±8.1
223Dis	15.1±6.7	12.2±5.6
101Dis	26.5±12.9	11.1±4.8
222Dis	4.9± 2.1	N/A
221Dis	14.4±6.4	4.8±3.3
50Disk	8.1±3.9	2.0±0.6
107Ext	9.6±7.8	N/A
w1old	9.0±6.5	N/A
167Hal	1.3±0.8	0.8±0.5
148Ext	1.1±0.9	0.7±0.5

assuming no contamination from residual sky lines and no covariance noise, where FWHM is the full width at half-maximum of the CaT lines which is typically 2–3 Å. Using this equation, we can determine the average errors in [Fe/H] for stars in our sample at different S:N, and we find that for spectra with S:N of (5, 8, 10) Å⁻¹, the errors in their calculated metallicity are of order (0.6, 0.4, 0.3) dex. To demonstrate the effects of these large errors on the metallicity distribution function (MDF) of our sample, we present histograms of the individual spectroscopic metallicities for three quality cuts, one at S:N ≥ 10 Å⁻¹ (left panel), one with S:N ≥ 8 Å⁻¹ (middle panel) and one with S:N ≥ 5 Å⁻¹ (right panel) in Fig. 11. In both plots, the blue hatched histogram represents our thin disc sample and the filled red histogram represents our thick disc population. For our higher quality spectra, we calculate a median metallicity for the thin disc of [Fe/H]=-0.9 with a dispersion of 0.4 dex (from the inter quartile range, IQR). For our thick disc population we calculate a median of [Fe/H]=-1.0 also with a dispersion of 0.4 dex. We note that the distributions of both populations deviate from a Gaussian distribution, with a kurtosis of -0.6 and -0.3 for thin and thick discs respectively, implying a broad peaked distribution, with narrow tails. Both distributions are skewed towards lower metallicity with skewness $\alpha = -0.4$ and $\alpha = -0.3$ for thin and thick disc. For our lowest S:N cut, however, much of this information is lost. While the median [Fe/H] remains very similar with [Fe/H]=-1.0 for the thin disc and [Fe/H]=-1.1 for the thick, the distributions begin to broaden, with dispersions of 0.5 dex for both populations, and present almost no skew ($\alpha = -0.1$ and $\alpha = -0.2$ for thin and thick disc). This shows that by including data with larger measurement errors, we wash out our MDF considerably, and lose any meaningful information. As a sanity check, we compare the MDF for all stars with S:N ≥ 10 Å⁻¹

with one for stars with $S:N \geq 15 \text{ \AA}^{-1}$, and find both the median values of $[\text{Fe}/\text{H}]$ and general distributions to be comparable. We note that by requiring such a high $S:N$ cut on our individual measurements of $[\text{Fe}/\text{H}]$, we bias our sample towards more metal-rich stars as these will have intrinsically stronger Ca II lines.

Owing to the large errors associated with these measurements, this analysis provides a crude indication of the metallicities of both discs, and so to get a more accurate estimate of the average metallicities of both populations we construct composite spectra for both components (using both the 2σ and Gaussian velocity cuts) by co-adding the individual spectra of all stars with $S:N > 3 \text{ \AA}^{-1}$, weighted by their $S:N$ values. The resulting $S:N$ of the composite is much greater than the individual spectra ($S:N \sim 60 - 100$ cf. $S:N \sim 3 - 25$), allowing a better fit to the CaII lines. We use a cut of $S:N > 3 \text{ \AA}^{-1}$ as below this the velocity uncertainties of our stars begin to significantly increase (as discussed in § 3). As we shift all spectra to the rest frame before co-adding, including spectra where the velocity is uncertain could smear out the Ca II lines, resulting in an over-estimate of $[\text{Fe}/\text{H}]$ for the composite. We note that the results from our composites are only indicative of an average metallicity for each component, and can tell us nothing about the metallicity dispersion for the discs. We display the resulting composites in Fig. 12. The top 2 panels show the thin and thick spectra for the 2σ velocity cuts, while the bottom 2 panels show the same, but for the Gaussian velocity cuts. In the case of the 2σ cuts, our thin composite comprises 511 stars that match our kinematic and quality criteria, while our thick composite is constructed from 78 stars. For our Gaussian cuts, these numbers fall to 380 and 52 stars respectively. We find an offset of order 0.2 dex between the thick and thin components for the 2σ cuts, with the thick disc being more metal poor at $[\text{Fe}/\text{H}] = -0.9 \pm 0.1$ compared with $[\text{Fe}/\text{H}] = -0.7 \pm 0.05$ for the thin, inconsistent within their respective 1σ errors. For our Gaussian cuts, we find the thick disc to be more metal poor, giving us a larger difference in metallicity between the two components of 0.3 dex (with $[\text{Fe}/\text{H}] = -1.0 \pm 0.1$ for the thick disc compared with $[\text{Fe}/\text{H}] = -0.7 \pm 0.05$ for the thin), although the two results for the thick disc are consistent within their 1σ errors. We also note that we are liable to experience non-negligible thin disc contamination of our thick disc component, which could cause us to over estimate the average $[\text{Fe}/\text{H}]$, so the true difference could be larger still. We note that these results are consistent with performing the same analysis on composites constructed from spectra with $S:N > 10 \text{ \AA}^{-1}$.

Finally, the continuum fit to the third line in our composite spectra, particularly for our thick disc selection, gives us some cause for concern. Could this metallicity difference we derive be driven by poor continuum fitting in this region of the spectrum? To investigate this, we analyse the $[\text{Fe}/\text{H}]$ for the thin and thick discs again, using solely the first two lines (CaII₈₄₉₈ and CaII₈₅₄₂). In the case of our simple 2σ cut, this narrows our difference in metallicity slightly from 0.2 dex to 0.15 dex, with $[\text{Fe}/\text{H}] = -0.85 \pm 0.1$ compared with $[\text{Fe}/\text{H}] = -0.7 \pm 0.05$ for the thick and thin discs respectively. However, in the case of our Gaussian cuts, which are arguably less affected by cross contamination between

the components, the metallicity difference of 0.3 dex persists.

We also perform this composite analysis on a field-by-field basis. The results of this analysis, shown in Table 2 are again, less accurate than our overall composite, but they suggest a similar offset in metallicity exists in the thin and thick components in each field. We plot this result as a function of radius in the lower panel of Fig. 8. We find no evidence for any evolution of metallicity with radius.

A slight concern in ascertaining the metallicity of a population from a composite spectrum arises from inaccuracies in the estimate that come from combining spectra with different effective temperatures and V -band magnitudes, as the derived metallicities are weakly dependent on the apparent V -band colours of the stars. The rms dispersion in the V -band magnitudes within our sample are small (< 0.5 mag for both thin and thick discs) as we are sampling only a small region of the tip of the RGB, so the error introduced by this effect will be very small. However, to further assess this, we separate our thin and thick disc spectra into bins of 0.2 mags in the V -band and create composite spectra for each bin, measuring the metallicity of each. We show a sample of these spectra in Fig. 13, labelled with the metallicity and average V -band magnitude. The typical errors in metallicities determined for these composites ranges from 0.1–0.3 dex. What we see is that the composite thick disc spectrum in each bin is more metal-poor than the corresponding thin disc composite. We also find that the average metallicities for both thin and thick discs agree with those that we derived from the composites for the entire sample.

4.3 Photometric Metallicities

We inspected the photometric metallicities of our sample using the Dartmouth isochrone models (Dotter et al. 2008). We select an age of 8 Gyrs as the work of Brown et al. (2006) suggests that the age of the disc in these outer regions varies between 4 and 8 Gyrs. We use an α -abundance of $[\alpha/\text{Fe}] = +0.2$ as it has been shown in various works (e.g. Reddy et al. 2006; Alves-Brito et al. 2010) that the α -enhancement of thin or extended stellar disc populations typically ranges between $[\alpha/\text{Fe}] = +0.0$ and $[\alpha/\text{Fe}] = +0.2$. We then interpolate between these isochrone models for every star within our sample to determine its metallicity. We can then compare the MDFs for our thin and thick disc sample, selected by both the 2σ and Gaussian cuts discussed above. The results of this are shown in the left panel of Fig. 14. This figure shows us that when using this set of isochrones, the MDFs of both populations trace each other remarkably well. We calculate a median metallicity for each component and find $[\text{Fe}/\text{H}]_{\text{thin}} = -0.79$ and $[\text{Fe}/\text{H}]_{\text{thick}} = -0.80$, both with IQRs of 0.2 dex. Neither population has a Gaussian distribution, with positive kurtosis of +2.2 for both MDFs (i.e. more peaked, with broader tails), and both populations are skewed towards lower $[\text{Fe}/\text{H}]$ with $\alpha \sim -1.2$ for both discs. From this analysis, one might conclude that the two discs are chemically indistinguishable. This is in contrast to our findings from the combined spectra in §4.2 where we find an offset in the average metallicities of thin and thick components of 0.2 dex. As our photometric data are not deep enough to detect the MSTO of these fields, we are exposed to the age-metallicity- $[\alpha/\text{Fe}]$ degeneracy problem. If we analyse

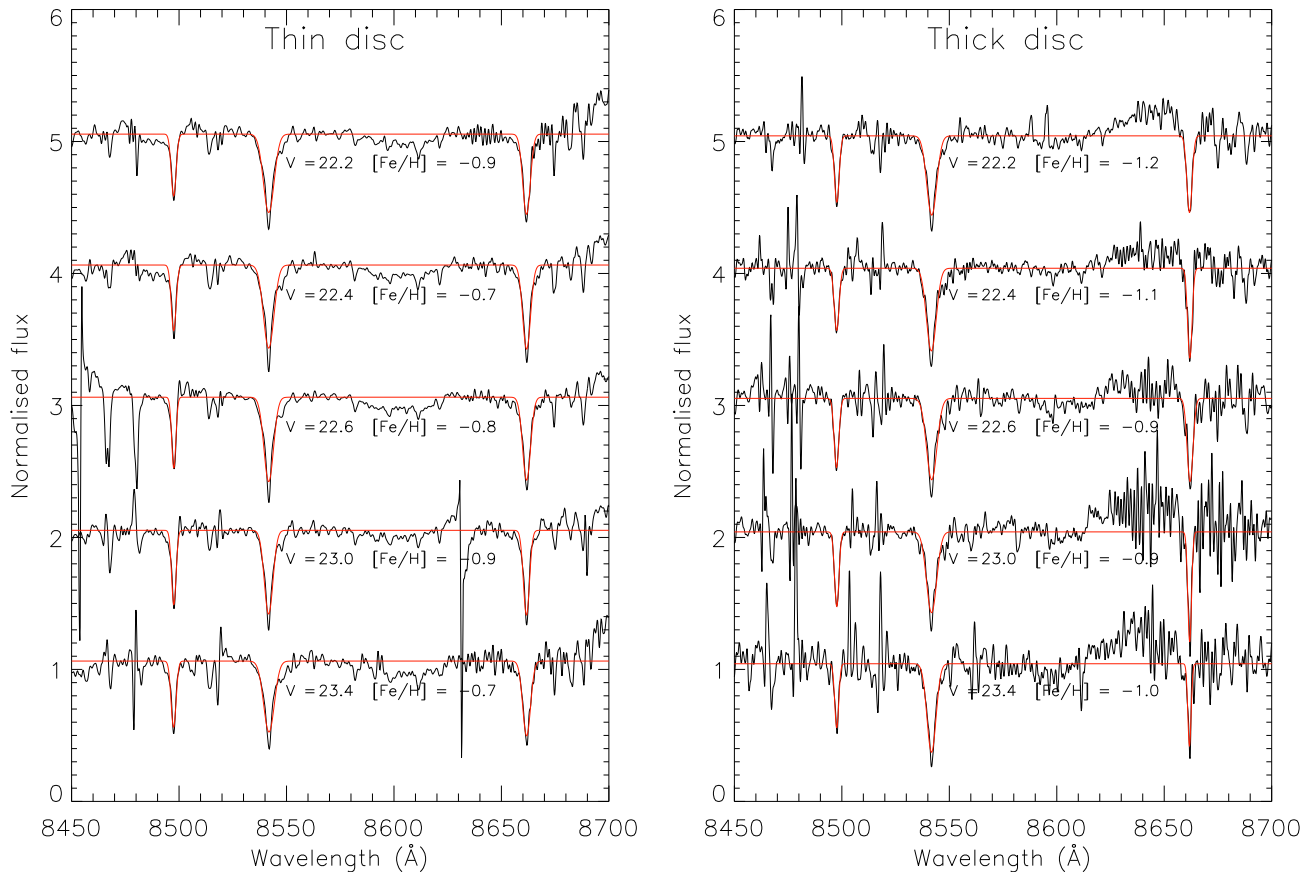


Figure 13. Composite spectra of our thin (left panel) and thick (right panel) disc samples, binned in V -band magnitude. Each bin spans 0.2 mags. We see that in each case, the thick disc is more metal-poor than the thin disc by ~ 0.2 dex. The errors in the values of $[\text{Fe}/\text{H}]$ for these composites ranges from 0.1–0.3 dex.

our data with isochrones of different ages and abundances, we find that the individual metallicities we measure change. Increasing the age by 2 Gyrs has the effect of decreasing $[\text{Fe}/\text{H}]$ of a star by ~ 0.05 dex on average (shown in the centre panel of Fig 14) and increasing the abundance from $[\alpha/\text{Fe}]=+0.2$ to $[\alpha/\text{Fe}]=+0.4$ reduces $[\text{Fe}/\text{H}]$ by ~ 0.1 dex, (right hand panel, Fig. 14). The dispersions, kurtosis and skew remain largely unchanged by these variations. These findings demonstrate that it may be difficult to discern slight differences in metallicity (such as the 0.2 dex measured in §4.2) using photometric isochrones without knowing the ages and/or α -abundances of the thick and thin disc. Studies of the thin and thick discs in the MW have shown that the thick disc is both older and more α -enriched than the thin disc (Reddy et al. 2006; Alves-Brito et al. 2010), and many of the formation scenarios of thick discs suggest this could be true for thick discs in general, including M31. Such differences would certainly affect our derived values of $[\text{Fe}/\text{H}]$ for both discs.

5 DISCUSSION

In this section we discuss our findings, and comment on the morphology of this thick component. First we compare our findings with an expected thin+thick disc population

inclined to us along the line of sight by 77° , by creating a model of a galaxy with a thin/extended disc with similar properties to those of M31 that has an additional thick disc component and analysing it in the same way as our data. We then compare the M31 thick disc to the MW and the Yoachim & Dalcanton (2006) sample of thick discs. Finally we comment on the possible formation mechanisms for this component.

5.1 Comparison with thin + thick disc model

To lend confidence to our defining the lagging component we isolate in the above analysis as a thick disc, we create a simple kinematic model of a galaxy with properties similar to those of a MW-type galaxy, which has both a thin and thick stellar disc, and analyse this in the same manner as our data. This is done as follows; first, we create a thin stellar disc of 9×10^6 stars, randomly generating radii for each assuming the stars are distributed in an exponential disc with a scale length equal to that of M31’s (6.6 kpc, I05). We assign each particle with a velocity randomly drawn from a Gaussian population centred on 0 km s^{-1} with a velocity dispersion of 25 km s^{-1} in the disc frame. We repeat this for our thick disc component, assuming a thin:thick disc density ratio in M31 that is equal to that measured in the solar

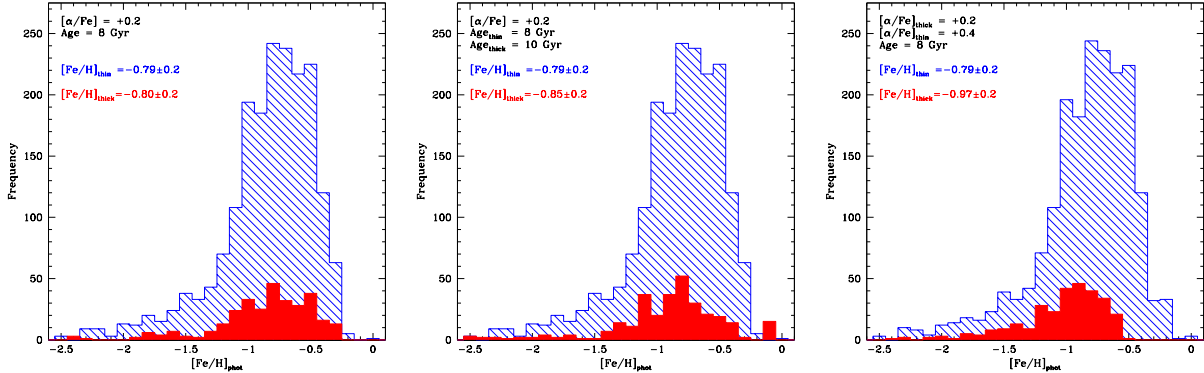


Figure 14. Photometric MDFs derived from Dartmouth isochrones of varying age and $[\alpha/\text{Fe}]$ (Dotter et al. 2008) for the thin and thick components (shown as blue hatched and red filled histograms respectively) as defined by our 2σ cuts. **Left panel:** Analysis of $[\text{Fe}/\text{H}]$ for thin and disc using $[\alpha/\text{Fe}] = +0.2$ and an age of 8 Gyrs. We detect no significant differences between the two populations, calculating median $[\text{Fe}/\text{H}]$ and $[\text{Fe}/\text{H}]_{\text{thick}} = -0.8 \pm 0.2$. **Centre panel:** Increasing the age of isochrones used to calculate metallicity for the thick disc from 8 Gyrs to 10 Gyrs. An offset of ~ 0.05 dex in the average $[\text{Fe}/\text{H}]$ of the two components is observed, with median $[\text{Fe}/\text{H}]_{\text{thick}} = -0.85$. The dispersion remains the same as before. **Right panel:** Increasing $[\alpha/\text{Fe}]$ for the thick disc from $+0.2$ to $+0.4$. An offset of ~ 0.1 dex between the median metallicities of the populations is now observed, with $[\text{Fe}/\text{H}]_{\text{thick}} = -0.93$.

neighbourhood of 9:1 (Just & Jahreiß 2010), giving 1×10^6 stars, and we use a thick disc scale length of 8.0 kpc, as determined above. For the velocities, we assume the thick disc lags behind the thin by 50 km s^{-1} and has the same velocity dispersion as the MW thick disc, $\sigma = 40 \text{ km s}^{-1}$ (Ivezić et al. 2008). We also generate vertical heights within the discs for both thin and thick populations, assuming MW scale heights for the discs (300 pc and 1000 pc for thin and thick disc, Ivezić et al. 2008), I -band magnitudes between $25.0 \geq I \geq 20.3$ (0.1 mags brighter than the tip of the RGB in M31) and angular positions within the disc. We then convert our disc frame velocities into heliocentric velocities using the HI rotation curve of Chemin et al. (2009). Finally, we interpret this model in the same way as our data, by rotating it into the coordinate system of M31 as observed from the MW (with inclination and PA as discussed in § 3), and subtracting off the assumed disc velocity at that position by interpolating each of our model stars into our average disc velocity map (Fig. 4).

From this model data set, we select stars as we would select targets to observe when designing DEIMOS masks, requiring them to have I -band magnitudes between $22.0 \geq I \geq 20.5$. We then randomly select the same number of stars as are observed at each field location, and make velocity histograms in the disc-lag frame for each field. We then analyse these distributions with the same GMM technique described in § 3.1, using a LRT to determine whether the distribution of each model field is best fit by a single thin disc component, or a double thin+thick component. This procedure is repeated 100 times, allowing us to compute the average velocities and dispersions for each component, plus sampling errors which we tabulate in Table 5. In our final 100 samples, the thick disc is detected in 15 of the 21 fields on average. The fact that we do not see the thick disc component in all our model fields implies that the non-detections in our data are an effect of our sampling of the DEIMOS fields rather than the component being absent in these fields. We show

the histograms and best fit Gaussians for three of these realizations compared to our data in Fig. 15.

We now assess how both the lag between components and the dispersions of each component evolve with radius for our model data set, and how accurately we can recover these values from our model. In Fig. 16, we plot these values for our model (black circles) alongside the values we obtained from our data (red squares), and fit the evolution of the model results with linear functions as before. In the top panel, we show the measurement of Δv for our model fields as a function of projected radius. The model results show no evolution of Δv with radius, recovering an average lag across all fields of $48.9 \pm 6.7 \text{ km s}^{-1}$, which is similar to the constant lag of 50 km s^{-1} implemented in our model.

Next, we compare the evolution of the disc dispersions for our model with the data, shown in the central and lower panels of Fig. 16. The model thin disc is best fit with a constant relation, giving an average lag of $\sigma_{\text{thin}} = 21.5 \pm 1.7 \text{ km s}^{-1}$, very close to the input of 25.0 km s^{-1} . For the thick disc dispersion, σ_{thick} the measured dispersion in the model scatters about a mean dispersion of $\sigma_{\text{thick}} = 38.8 \pm 2.4 \text{ km s}^{-1}$, with no evidence of evolution with radius.

Finally, we can use our model to get a handle on how accurate our estimates of the scale length of the M31 discs might be. We use the same Monte Carlo (MC) technique above to calculate the density of stars in each component in our model fields 100 times, then we compute the average density from these results. These results are shown in Table 6, and the errors represent the dispersion of the densities computed in each field. We then plot the densities as a function of radius for the thin and thick discs (shown in Fig. 17), and fit the result with an exponential profile to determine the scale length. For the thin disc, we calculate $h_r = 6.2 \pm 0.8 \text{ kpc}$, which is consistent with our input of 6.6 kpc, and for the thick disc we compute $h_r = 7.8 \pm 0.9 \text{ kpc}$, consistent with our input of 8.0 kpc. The shaded regions indicate the 1σ uncertainties from the fit. These results suggest that our observationally derived scale lengths for the

Table 5. Average kinematic properties of model fields from 100 MC realisations

Field	v_{thin} (disc frame, km s^{-1})	σ_{thin} (km s^{-1})	v_{thick} (disc frame, km s^{-1})	σ_{thick} (km s^{-1})
228Mod	11.4±5.0	19.2±8.0	-50.0±8.9	38.3±8.1
227Mod	-1.7±0.6	25.5±10.8	-37.1±15.6	46.3±12.4
166Mod	-3.4±2.1	25.9±7.3	-46.3±9.1	43.0±13.4
106Mod	-4.4±3.2	25.9±8.2	-54.3±14.1	42.8±9.3
105Mod	-2.1±1.2	22.0±9.4	-54.6±13.8	39.4±12.8
224Mod	-2.7±1.9	23.1±9.9	-40.2±9.2	42.3±10.3
232Mod	-3.1±2.7	21.8±8.2	-45.9±12.2	41.2±13.2
104Mod	-2.5±1.7	22.8±10.2	-57.6±14.4	43.0±11.0
220Mod	-7.0±3.8	21.1±10.3	-62.9±8.7	36.2±10.4
213Mod	-8.1±4.3	19.5±9.9	-55.1±13.2	32.2±13.9
102Mod	-3.5±2.7	20.6±8.9	-49.1±7.9	34.9±12.4
231Mod	-3.7±2.2	19.4±7.4	-49.6±12.3	33.2±9.3
223Mod	-1.8±1.1	20.8±7.2	-56.1±11.7	36.7±8.8
101Mod	1.9±1.3	22.3±7.0	-64.1±11.2	38.4±10.8
222Mod	-0.1±1.2	19.9±6.6	-51.3±12.6	34.8±11.0
221Mod	3.9±2.3	19.9±8.6	-46.2±7.0	38.1±11.1
50Mod	4.2±2.5	17.9±8.2	-42.2±15.5	33.5±12.6
107Mod	5.1±2.7	17.5±7.7	-57.1±11.6	40.4±12.9
w11Mod	4.7±1.1	19.5±6.8	-63.1±10.4	43.4±10.5
167Mod	2.0±0.7	22.5±5.7	-52.2±8.6	41.6±9.7
148Mod	-1.2±1.5	25.2±6.8	-53.2±9.7	36.5±10.3

Table 6. Average densities for thin and thick discs in model fields from 100 MC realisations

Field	ρ_{*thin} (* / arcmin)	ρ_{*thick} (* / arcmin)
228Mod	73.0±35.2	31.0± 19.2
227Mod	15.7 ± 7.1	18.4 ± 8.1
166Mod	14.2 ± 7.7	14.1 ± 7.7
106Mod	11.9 ± 5.7	11.8 ± 5.7
105Mod	13.5 ± 6.3	10.8 ± 5.3
224Mod	10.6 ± 5.0	10.1 ± 4.8
232Mod	10.9 ± 6.1	7.6 ± 4.5
104Mod	10.7 ± 4.9	7.9 ± 3.8
220Mod	4.7 ± 1.8	4.2 ± 1.6
213Mod	4.6 ± 2.6	4.4 ± 2.4
102Mod	3.7 ± 1.5	3.8 ± 1.5
231Mod	3.8 ± 1.9	2.8 ± 1.3
223Mod	2.7 ± 1.0	2.7 ± 0.9
101Mod	2.9 ± 1.1	2.8 ± 1.0
222Mod	2.1 ± 0.7	2.1 ± 0.6
221Mod	1.7 ± 0.5	1.9 ± 0.5
50Mod	1.3 ± 0.3	1.2 ± 0.2
107Mod	1.4 ± 0.3	1.5 ± 0.3
w11Mod	1.4 ± 0.4	1.5 ± 0.3
167Mod	0.7 ± 0.4	0.5 ± 0.4
148Mod	0.6 ± 0.4	0.5 ± 0.3

thin and thick discs are a good indicator of their true scale lengths.

5.2 Comparison to the MW and ‘edge-on’ thick discs

Now that we have characterised the radial profile, kinematics and metallicity of the thick disc in M31, we are able to compare it to the properties of other thick discs that have been observed in the universe. We shall begin with the most well

studied thick disc currently known – that of our own Galaxy. Given that these two galaxies are relatively close to one another (separated by 785 kpc), and have similar morphologies (both large spiral galaxies), comparisons between the MW and M31 are often made. But for all their apparent similarities, these two galaxies are quite different from one another. Work by Hammer et al. (2007) has shown that the MW is quite different in terms of its structure and evolutionary history from the majority of local spiral galaxies, whereas M31 is actually quite “typical”, so these differences are perhaps unsurprising. In this work, we have demonstrated that the scale lengths of the M31 discs are larger than those of the MW by a factor of ~ 2 , as shown in Fig. 10. Given that we derive the scale heights of the M31 discs from these scale lengths, this results in scale heights in M31 that are of order ~ 3 times as thick as those of the MW. However, we note that as we calculate scale heights for the M31 disc based on a relation determined from disc galaxies that are quite different in terms of their mass to both the MW and M31, our values may be an overestimate. The M31 discs are also seemingly hotter than the MW discs, with $\sigma_{thin,M31} = 32.0 \text{ km s}^{-1}$ cf. $\sigma_{thin,MW} = 20.0 \text{ km s}^{-1}$ (Ivezić et al. 2008), and $\sigma_{thick,M31} = 45.7 \text{ km s}^{-1}$ cf. $\sigma_{thick,MW} = 40.0 \text{ km s}^{-1}$ (Ivezić et al. 2008). This could tell us something about the merger history of M31. If the thick discs in both galaxies are formed as a result of heating by mergers, the hotter discs of M31 could imply that this galaxy has undergone a more active merger history than the MW.

The MW thick disc is more metal poor, enriched in α metals and older than the thin disc. While we are unable to measure the age and α abundances of the M31 discs, we have shown that there exists an offset in the average metallicities of the two components of ~ 0.2 dex when measured spectroscopically. While we do not see this offset photometrically, this could be due to our analysis technique as we use isochrones of the same α abundance ($[\alpha/\text{Fe}] = +0.2$)

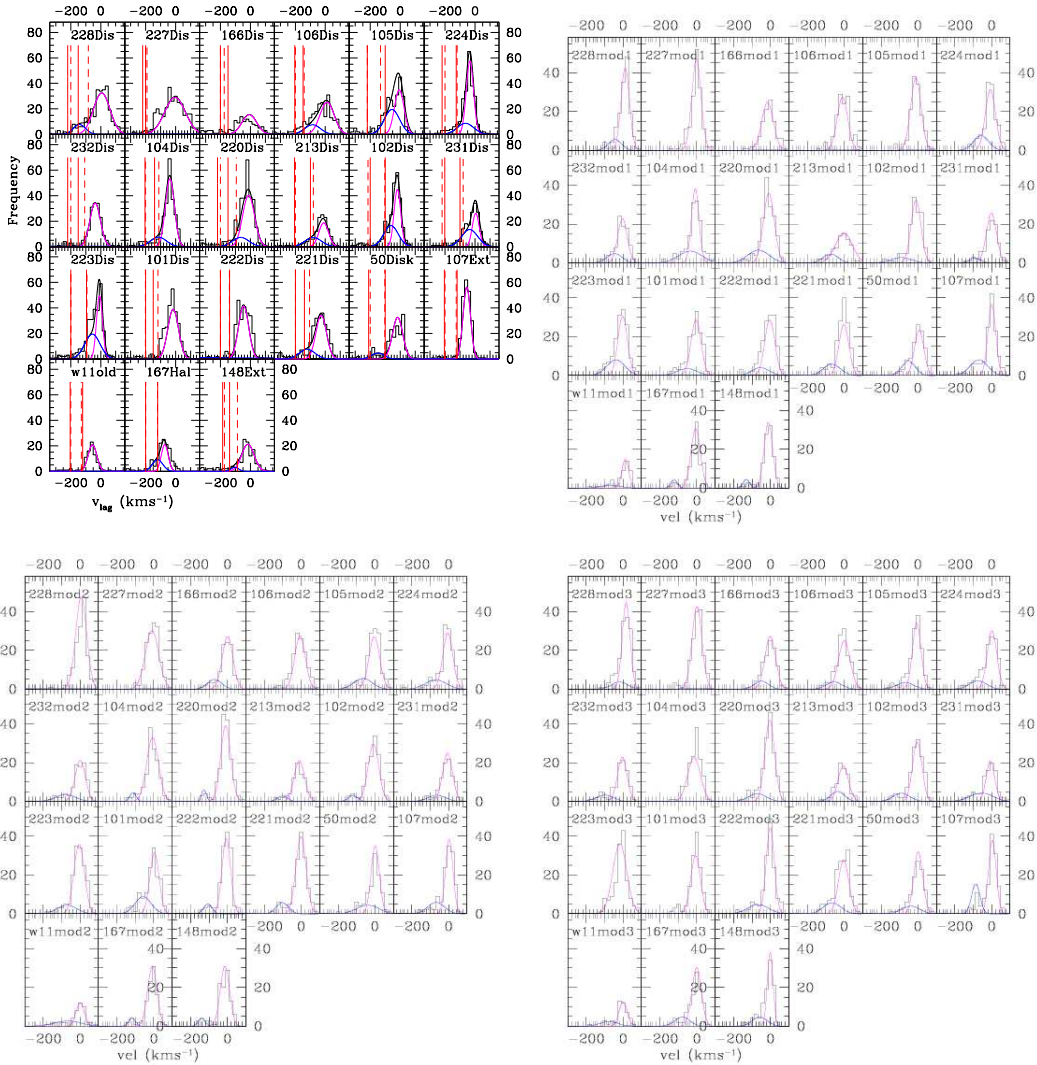


Figure 15. A comparison of the data (top left panel) with 3 realisations of parsing our thin + thick disc model through the same analysis as our data, selecting stars from the same regions as the data. It can be seen that the model data resembles the actual data very closely, and that non-detections are likely an effect of sampling.

and age (8 Gyrs) for both components. If we modify the α -abundance and age of these isochrones to $[\alpha/\text{Fe}] = +0.4$ and 10 Gyrs for our thick disc sample, we see an offset of ~ 0.2 dex. We also note that both the thin and thick discs in M31 appear to be more metal-poor than the MW discs, which have average metallicities of $[\text{Fe}/\text{H}] \sim -0.3$ and $[\text{Fe}/\text{H}] \sim -0.6$ (Gilmore et al. 2002; Abadi et al. 2003; Carollo et al. 2010) respectively, although there is a significant metallicity spread in both discs. Carollo et al. (2010) also demonstrated evidence of a secondary, more metal poor thick disc in the MW, whose metallicities span the range $-1.8 \leq [\text{Fe}/\text{H}] \leq -0.8$, peaking at $[\text{Fe}/\text{H}] = -1.3$. This component also appears to be hotter than the traditional MW thick disc component, with $\sigma_z = 44 \pm 3 \text{ km s}^{-1}$, very similar to what we observe in M31.

In §4.1.3, we inferred scale heights for the thin and thick discs of M31 of $h_z = 1.1 \pm 0.2 \text{ kpc}$ and $h_z = 2.8 \pm 0.6 \text{ kpc}$ respectively, using a sample of 34 galaxies with thick discs measured by YD06 to determine a relationship between scale

length and scale height of a stellar disc. As we noted in §4.1.3, a comparison with the YD06 sample might not be desirable, as these galaxies are typically much less massive than M31, and selected to be bulgeless. A more appropriate comparison would be the MW analogue, NGC 891, an edge-on galaxy that was recently the subject of a structural analysis by Ibata et al. (2009) using HST/ACS imaging. They detected the presence of a thick disc component in the galaxy and were able to measure both a scale length and height for this component of $h_r = 4.8 \pm 0.1 \text{ kpc}$ and $z_0 = 1.44 \pm 0.03 \text{ kpc}$, compared with $h_r = 4.2 \pm 0.01 \text{ kpc}$ and $z_0 = 0.57 \pm 0.01 \text{ kpc}$ for the thin disc component in this galaxy. This gives a ratio of ~ 1.1 between the scale lengths and ~ 2.5 for the scale heights of these components, which is identical to what we observe in M31. To illustrate this, we overplot these values for NGC 891 in Fig. 9 as a green circle.

In Yoachim & Dalcanton (2008b) the authors present kinematics of the thin and thick discs of 9 of their initial sample of 34 galaxies, obtained using the GMOS spectro-

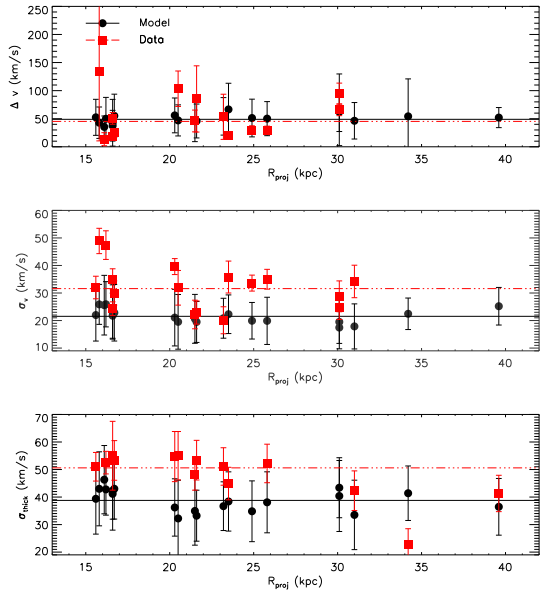


Figure 16. This figure compares the results from our data with results from our model analysed in the same way. In all cases, data is represented by filled red squares and dot-dashed lines, and the model results are shown as filled black circles and solid lines. **Top panel:** The difference in velocity, Δv , between the thin disc and thick component of data and model as a function of projected radius. The model lag is consistent with no evolution with radius, and shows an average lag of 48.9 km s^{-1} , very close to our input lag of 50 km s^{-1} . **Middle panel:** Dispersion, σ_{thin} , of the thin disc is plotted for both data and model as a function of projected radius. The model thin disc is best fit with an average dispersion of 21.5 km s^{-1} , very close to the input of 25.0 km s^{-1} . **Lower panel** Results for both data and model for the dispersion of the thick disc (σ_{thick}) as a function of radius. For our model, the thick disc is consistent with no evolution with radius, unlike our data, and has an average dispersion of $\sigma_v = 38.8 \text{ km s}^{-1}$, which recovers our input dispersion of 40 km s^{-1} relatively well.

graph on Gemini. To measure velocities and dispersions in both thin and thick components, they placed slits in positions corresponding to the midplane of the galaxy to measure the thin disc properties, and above the midplane where the contribution from the thin disc was thought to be negligible. As their typical velocity resolution was 60 km s^{-1} , they were unable to draw robust conclusions on the velocity dispersions of these components, but they were able to measure velocity rotation curves for each component, and found a wide variety of behaviour amongst their thick disc components, with discs which lagged behind the thin disc by only $\sim 5 \text{ km s}^{-1}$, discs that show no evidence of rotation and one case where the thick disc is counter-rotating with respect to the thin disc. The average lag between the thin and thick components of $\Delta v = 46.0 \text{ km s}^{-1}$ we see in the M31 system is larger than the majority that they observe. We note that the galaxies in their sample were typically of much lower mass than M31 ($V_{circ} < 150 \text{ km s}^{-1}$ cf $V_{circ} \sim 230 \text{ km s}^{-1}$). In the most massive of their sample (which are still less massive than M31), they do not detect a lag in the thick disc kinematics at all, and they attribute this to contrast issues. Their sample were also selected to be

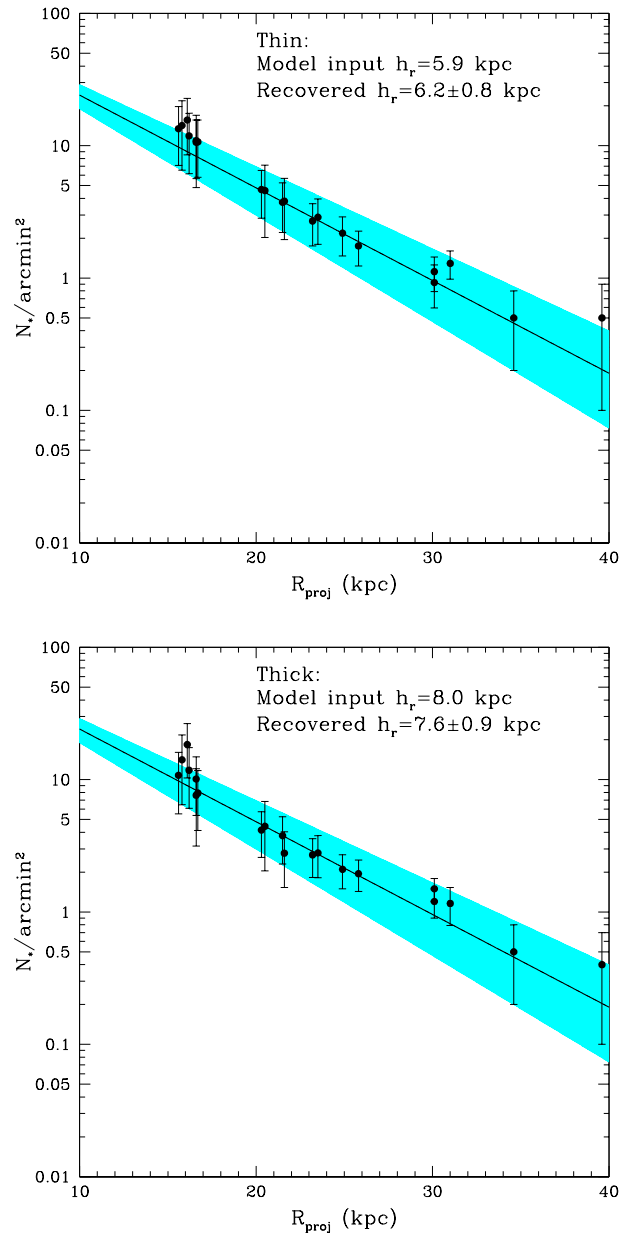


Figure 17. Results from MC recovery of the scale lengths in our thin+thick disc model for our input thin (top panel) and thick (bottom panel) discs. The error bars on individual points represent the dispersion of calculated densities in the MC analysis, while the shaded regions represent the 1σ uncertainties from the weighted least-squares fit. We recover a scale length for the thin disc of $h_r = 6.2 \pm 0.8 \text{ kpc}$ and $h_r = 7.6 \pm 0.9$ for the thick disc, which are consistent with our input values.

“bulgeless”, unlike M31 which has a significant bulge, and so a direct comparison may not be advisable. Owing to the wide range of kinematic behaviour exhibited in their sample, they conclude that the dominant formation process of thick discs is via minor mergers and accretions of satellites. In Yoachim & Dalcanton (2008a), they use Lick indices to measure ages and metallicities in 9 low mass galaxies with thick disc components. While we measure an offset of 0.2 dex

in the metallicities of the M31 thick and thin discs, they were unable to measure any such offset in their sample, though this could be a result of the insensitivity of Lick indices to such differences at low metallicity. They do find that the thick discs are host to older stellar populations than the thin disc, however with our current data set, we are unable to comment on the ages of stars in the M31 discs.

5.3 Possible formation scenarios

In this section, we discuss the various formation scenarios mentioned in § 1. Owing to our inability to measure ages and vertical dispersions in M31, we are not able to confirm or reject any of these formation mechanisms at present, so we discuss additional constraints for these models that could help to rule out or confirm each scenario with further data and analysis.

5.3.1 Heating by minor mergers

Numerous studies have identified that impacts and mergers of satellites with masses less than a third of their hosts can kinematically heat the thin stellar disc, puffing it out into a substantially thicker disc (e.g. Quinn et al. 1993; Robin et al. 1996; Walker et al. 1996; Velazquez & White 1999; Chen et al. 2001; Sales et al. 2009; Villalobos & Helmi 2009). M31 is known to have recently undergone at least one significant minor merger event, resulting in the GSS tidal stream. In recent work by Purcell et al. (2010), the authors model the heating of the stellar discs by minor mergers and trace disc stars ejected into the stellar halo by these simulated events. In addition to the stars ejected into the halo, they observe a concomitant increase in the number of stars located in the kinematic regime of the thick disc, contributing $\sim 10 - 20\%$ of the total stellar density along the major axis, similar to what we observe in M31. They also find that their simulated planar infall produces two-component systems with scale heights ($z_{thin} \sim 1$ kpc and $z_{thick} \sim 3$ kpc), consistent with our measurements for M31. The similarities between our findings and those of Purcell et al. (2010) could suggest that thin disc stars heated by the merging event that created the GSS may contribute some non-trivial fraction of stars to the thick disc.

According to the simulations of Kazantzidis et al. (2009), thick discs produced in this vein imprint a number of dynamical signatures on both the kinematic and structural properties of the galaxy. These include considerable thickening and heating at all radii, prominent flaring, particularly in the outskirts of the disc (beyond 3 scale lengths), surface density excesses at large radii, radial anisotropies and substantial tilting of the disc. As M31 is not edge on, we are unable to comment on the evolution of the height of the thick disc with radius, and so we cannot use this as a measure of flaring in the outer regions of the disc. However, one might expect that if there was a substantial flaring beyond 3 disc scale lengths (~ 24 kpc), that this may be reflected by an increase in the velocity dispersions of both thin and thick disc components. Our results for evolution in the thin and thick disc dispersions remain inconclusive, and so it is possible that such flaring may exist. At present, we possess few fields between $R \sim 32$ and 39.6 kpc, so populating this region with kinematics, as well as additional fields further out,

may further enlighten us to any potential flaring. Another test of this formation scenario would be to include fields from both the minor axis and NE portion of M31 to test for any radial anisotropy, assuming one can reliably disentangle contamination from foreground and substructure from the signatures of the discs. The work of Sales et al. (2009) also tells us that thick discs that are produced as a result of heating present structures with low orbital eccentricity.

5.3.2 Accretion of satellite on a coplanar orbit

Numerical simulations by Abadi et al. (2003) and Peñarrubia et al. (2006) show that an old, thick disc of stars could form via the accretion of stars from satellite galaxies on an approximately coplanar orbit with its host. Such discs are similar in radial extent and contain older stellar populations when compared to the thin disc. The thick disc we find in M31 is consistent with this model in so far as the radial extents of both discs ($5.9 - 7.3$ kpc and 8.0 kpc) are comparable with one another. They also argue that the mass and luminosity of the progenitor satellite can be inferred from the metallicity of the component. We deduce $[\text{Fe}/\text{H}]_{thick} = -1.0 \pm 0.1$ for M31, which would correspond to a satellite of $M_V \sim -15$ ($L_V \sim 9 \times 10^7 L_\odot$), similar to the M31 dwarf elliptical, NGC 147 ($M_V = -15.1$, van den Bergh 1999). However, given the mass we calculate for the thick disc in §4.1.4 of $2 - 4 \times 10^{10} M_\odot$, it seems very unlikely that the thick disc of M31 could have been formed from such a satellite.

Results of the simulations of Sales et al. (2009) show that stars accreted into a thick disc from satellites on coplanar orbits exhibit high eccentricity orbits. Our present data set does not allow us to probe the eccentricity of the orbits within the thick disc at this time. With a larger data set, we could perhaps see the effects of orbital differences in the form of structural asymmetries.

5.3.3 Radial migration and internal heating

The scattering of stars by spiral structure and molecular clouds has long been proposed as a method of heating the stellar disc, moving stars out onto more eccentric and inclined orbits (Sellwood & Binney 2002; Haywood 2008; Roškar et al. 2008; Schönrich & Binney 2009a), and it has been argued in Schönrich & Binney (2009a,b) that these processes naturally produce an old, α -enhanced thick disc, whose properties are consistent with those observed in the MW. These models also show wide MDFs and an increase in the scatter of the Age-Metallicity relation. This is also demonstrated in Quillen et al. (2009), where they investigate radial mixing induced by an orbiting subhalo. Again they find evidence of wide MDFs in both the thin and thick discs. With deeper photometry that allowed us to reach the MSTOs of the two discs we could derive the average ages of these components, and high resolution spectroscopy ($R \sim 15,000$) of M31 thick disc stars that would allow us to determine accurate abundances from unblended Fe lines for individual stars, we could comment more robustly on the likelihood of such a formation scenario.

5.3.4 Thick disc forms thick

Kroupa (2002) posited that thick discs could be formed as a result of vigorous star formation in massive star clusters ($\sim 10^5 - 10^6 M_\odot$) during the period of assembly of the stellar disc. If this is true, a number of these massive clusters may have survived to the present day, and would possess large vertical velocity dispersions. Kroupa (2002) suggests that these clusters could be the metal-rich globular cluster system in the MW. Once again, owing to the inclination of M31, we are unable to measure the vertical dispersions of its metal-rich globular cluster system, and can therefore neither confirm nor reject this formation model.

6 CONCLUSIONS

Using the DEIMOS spectrograph on the Keck II telescope, we have identified a statistically significant population of stars in M31 that lags behind the thin and extended discs by $46.0 \pm 3.9 \text{ km s}^{-1}$. Comparing this with a model of a thin+thick disc system with the same distance and inclination as M31 shows this component to be consistent with a thick disc component. Analysing its kinematics, we find it to be hotter than the thin disc, with average dispersion $\sigma_{thick} = 50.8 \pm 1.9 \text{ km s}^{-1}$ cf. $\sigma_{thin} = 35.7 \pm 1.0 \text{ km s}^{-1}$, larger than the dispersions observed in the MW discs. From composite spectra for each component, constructed from highly probable thin and thick disc stars (selected using stringent Gaussian cuts) we measure a metallicity offset of ~ 0.3 dex between the two disc, with the thick disc being metal-poor than the thin disc ($[\text{Fe}/\text{H}]_{thick} = -1.0 \pm 0.1$ cf. $[\text{Fe}/\text{H}]_{thin} = -0.7 \pm 0.05$). The fact that this metallicity offset is not observed when analysing the thin and thick disc RGB stars with isochrones of identical age and α -abundance suggests that the two populations differ in these properties, with the thick disc likely being older and more enriched in α elements.

We measure scale lengths for both thin and thick discs, finding $h_r = 8.0 \pm 1.2 \text{ kpc}$ for the thick disc, and $h_r = 7.3 \pm 1.1 \text{ kpc}$ for the thin disc, comparable to previous estimates. Using the data of YD06 we infer scale heights for both discs at $z_0 = 2.8 \pm 0.6 \text{ kpc}$ and $z_0 = 1.1 \pm 0.2 \text{ kpc}$ for thick and thin discs respectively. These values are of order 2–3 times larger than those measured in the MW, perhaps suggesting that M31 has undergone more heating than our Galaxy.

By measuring the ratio of the densities of both discs, we are able to estimate a mass range for the thick disc component of $2.4 \times 10^{10} M_\odot < M_{*,thick} < 4.1 \times 10^{10} M_\odot$. This value provides a useful constraint on possible formation mechanisms, as any proposed method for forming a thick disc must be able to heat (or deposit) at least this amount of material.

Owing to current limitations within our data set, we are not able to distinguish between the different thick disc formation mechanisms. However, with further analysis of this component using our complete kinematic sample (including regions from the minor axis and NE of M31) and spectroscopic follow up of fields where this component is strongly observed, we will be able to better understand the chemistry of this component and distinguish between various formation mechanisms.

7 ACKNOWLEDGEMENTS

MLMC would like to acknowledge the support of an STFC studentship. GFL acknowledges the award of the Cambridge Raymond & Beverly Sackler distinguished visitor fellowship.

REFERENCES

- Abadi M. G., Navarro J. F., Steinmetz M., Eke V. R., 2003, *ApJ*, 597, 21
- Alves-Brito A., Meléndez J., Asplund M., Ramírez I., Yong D., 2010, *A&A*, 513, A35+
- Ashman K. M., Bird C. M., Zepf S. E., 1994, *AJ*, 108, 2348
- Battaglia G., Irwin M., Tolstoy E., Hill V., Helmi A., Letarte B., Jablonka P., 2008, *MNRAS*, 383, 183
- Bensby T., Alves-Brito A., Oey M. S., Yong D., Meléndez J., 2010, *A&A*, 516, L13+
- Benson A. J., Lacey C. G., Frenk C. S., Baugh C. M., Cole S., 2004, *MNRAS*, 351, 1215
- Bournaud F., Elmegreen B. G., Martig M., 2009, *ApJ*, 707, L1
- Braun R., Thilker D. A., Walterbos R. A. M., Corbelli E., 2009, *ApJ*, 695, 937
- Brinks E., Burton W. B., 1984, *A&A*, 141, 195
- Brook C., Richard S., Kawata D., Martel H., Gibson B. K., 2007, *ApJ*, 658, 60
- Brook C. B., Kawata D., Gibson B. K., Freeman K. C., 2004, *ApJ*, 612, 894
- Brooks A. M., Governato F., Quinn T., Brook C. B., Wadsley J., 2009, *ApJ*, 694, 396
- Brown T. M., Smith E., Ferguson H. C., Rich R. M., Guhathakurta P., Renzini A., Sweigart A. V., Kimble R. A., 2006, *ApJ*, 652, 323
- Burstein D., 1979, *ApJ*, 234, 829
- Carlberg R. G., 1987, *ApJ*, 322, 59
- Carollo D., Beers T. C., Chiba M., Norris J. E., Freeman K. C., Lee Y. S., Ivezić Ž., Rockosi C. M., Yanny B., 2010, *ApJ*, 712, 692
- Cash W., 1979, *ApJ*, 228, 939
- Chapman S. C., Ibata R., Irwin M., Koch A., Letarte B., Martin N., Collins M., Lewis G. F., McConnachie A., Peñarrubia J., Rich R. M., Trethaway D., Ferguson A., Huxor A., Tanvir N., 2008, *MNRAS*, 390, 1437
- Chapman S. C., Ibata R., Lewis G. F., Ferguson A. M. N., Irwin M., McConnachie A., Tanvir N., 2005, *ApJ*, 632, L87
- Chapman S. C., Ibata R., Lewis G. F., Ferguson A. M. N., Irwin M., McConnachie A., Tanvir N., 2006, *ApJ*, 653, 255
- Chapman S. C., Peñarrubia J., Ibata R., McConnachie A., Martin N., Irwin M., Blain A., Lewis G. F., Letarte B., Lo K., Ludlow A., O’neil K., 2007, *ApJ*, 662, L79
- Chemin L., Carignan C., Foster T., 2009, *ApJ*, 705, 1395
- Chen B., Stoughton C., Smith J. A., Uomoto A., Pier J. R., Yanny B., Ivezić Ž., York D. G., Anderson J. E., Annis J., Brinkmann J., Csabai I., Fukugita M., Hindsley R., Lupton R., Munn J. A., the SDSS Collaboration 2001, *ApJ*, 553, 184
- Chen Y. Q., Zhao G., Zhao J. K., 2009, *ApJ*, 702, 1336
- Chiba M., Beers T. C., 2000, *AJ*, 119, 2843
- Choi P. I., Guhathakurta P., Johnston K. V., 2002, *AJ*, 124, 310

- Choi Y., Park C., Vogeley M. S., 2007, *ApJ*, 658, 884
- Collins M. L. M., Chapman S. C., Irwin M., Ibata R., Martin N. F., Ferguson A. M. N., Huxor A., Lewis G. F., Mackey A. D., McConnachie A. W., Tanvir N., 2009, *MNRAS*, 396, 1619
- Collins M. L. M., Chapman S. C., Irwin M. J., Martin N. F., Ibata R. A., Zucker D. B., Blain A., Ferguson A. M. N., Lewis G. F., McConnachie A. W., Peñarrubia J., 2010, *MNRAS*, 407, 2411
- Corbelli E., Lorenzoni S., Walterbos R., Braun R., Thilker D., 2010, *A&A*, 511, A89+
- Dalcanton J. J., Bernstein R. A., 2002, *AJ*, 124, 1328
- de Jong J. T. A., Yanny B., Rix H., Dolphin A. E., Martin N. F., Beers T. C., 2010, *ApJ*, 714, 663
- Delgado-Serrano R., Hammer F., Yang Y. B., Puech M., Flores H., Rodrigues M., 2010, *A&A*, 509, A78+
- Dotter A., Chaboyer B., Jevremovic D., Kostov V., Baron E., Ferguson J. W., 2008, *ArXiv e-prints*, 0804.4473
- Dubinski J., Gauthier J., Widrow L., Nickerson S., 2008, in J. G. Funes & E. M. Corsini ed., *Astronomical Society of the Pacific Conference Series Vol. 396 of Astronomical Society of the Pacific Conference Series, Spiral and Bar Instabilities Provoked by Dark Matter Satellites*. pp 321+
- Elmegreen B. G., Elmegreen D. M., 2006, *ApJ*, 650, 644
- Ferguson A. M. N., Irwin M. J., Ibata R. A., Lewis G. F., Tanvir N. R., 2002, *AJ*, 124, 1452
- Ferguson A. M. N., Johnson R. A., 2001, *ApJ*, 559, L13
- Geehan J. J., Fardal M. A., Babul A., Guhathakurta P., 2006, *MNRAS*, 366, 996
- Geha M., Guhathakurta P., Rich R. M., Cooper M. C., 2006, *AJ*, 131, 332
- Gilbert K. M., Guhathakurta P., Kalirai J. S., Rich R. M., Majewski S. R., Ostheimer J. C., Reitzel D. B., Cenarro A. J., Cooper M. C., Luine C., Patterson R. J., 2006, *ApJ*, 652, 1188
- Gilbert K. M., Guhathakurta P., Kollipara P., Beaton R. L., Geha M. C., Kalirai J. S., Kirby E. N., Majewski S. R., Patterson R. J., 2009, *ApJ*, 705, 1275
- Gilmore G., Reid N., 1983, *MNRAS*, 202, 1025
- Gilmore G., Wyse R. F. G., Norris J. E., 2002, *ApJ*, 574, L39
- Hammer F., Flores H., Elbaz D., Zheng X. Z., Liang Y. C., Cesarsky C., 2005, *A&A*, 430, 115
- Hammer F., Puech M., Chemin L., Flores H., Lehnert M. D., 2007, *ApJ*, 662, 322
- Hänninen J., Flynn C., 2002, *MNRAS*, 337, 731
- Hayashi H., Chiba M., 2006, *PASJ*, 58, 835
- Haywood M., 2008, *MNRAS*, 388, 1175
- Holland S., Fahlman G. G., Richer H. B., 1996, *AJ*, 112, 1035
- Hopkins P. F., Cox T. J., Younger J. D., Hernquist L., 2009, *ApJ*, 691, 1168
- Hopkins P. F., Hernquist L., Cox T. J., Younger J. D., Besla G., 2008, *ApJ*, 688, 757
- Howley K. M., Geha M., Guhathakurta P., Montgomery R. M., Laughlin G., Johnston K. V., 2008, *ApJ*, 683, 722
- Ibata R., Chapman S., Ferguson A. M. N., Lewis G., Irwin M., Tanvir N., 2005, *ApJ*, 634, 287
- Ibata R., Irwin M., Lewis G., Ferguson A. M. N., Tanvir N., 2001, *Nature*, 412, 49
- Ibata R., Martin N. F., Irwin M., Chapman S., Ferguson A. M. N., Lewis G. F., McConnachie A. W., 2007, *ApJ*, 671, 1591
- Ibata R., Mouhcine M., Rejkuba M., 2009, *MNRAS*, 395, 126
- Irwin M. J., Ferguson A. M. N., Ibata R. A., Lewis G. F., Tanvir N. R., 2005, *ApJ*, 628, L105
- Ivezić Ž., et al., 2008, *ApJ*, 684, 287
- Jurić M., et al., 2008, *ApJ*, 673, 864
- Just A., Jahreiß H., 2010, *MNRAS*, 402, 461
- Kalirai J. S., Beaton R. L., Geha M. C., Gilbert K. M., Guhathakurta P., Kirby E. N., Majewski S. R., Ostheimer J. C., Patterson R. J., Wolf J., 2010, *ApJ*, 711, 671
- Kalirai J. S., Gilbert K. M., Guhathakurta P., Majewski S. R., Ostheimer J. C., Rich R. M., Cooper M. C., Reitzel D. B., Patterson R. J., 2006, *ApJ*, 648, 389
- Kazantzidis S., Zentner A. R., Kravtsov A. V., 2006, *ApJ*, 641, 647
- Kazantzidis S., Zentner A. R., Kravtsov A. V., Bullock J. S., Debattista V. P., 2009, *ApJ*, 700, 1896
- Klypin A., Zhao H., Somerville R. S., 2002, *ApJ*, 573, 597
- Koch A., Wilkinson M. I., Kleyna J. T., Irwin M., Zucker D. B., Belokurov V., Gilmore G. F., Fellhauer M., Evans N. W., 2008, *ArXiv e-prints*
- Kormendy J., Bender R., 1999, *ApJ*, 522, 772
- Kroupa P., 2002, *MNRAS*, 330, 707
- Loebman S. R., Roskar R., Debattista V. P., Ivezić Z., Quinn T. R., Wadsley J., 2010, *ArXiv e-prints*
- McConnachie A. W., et al., 2009, *Nature*, 461, 66
- McConnachie A. W., Irwin M. J., Ferguson A. M. N., Ibata R. A., Lewis G. F., Tanvir N., 2004, *MNRAS*, 350, 243
- McConnachie A. W., Irwin M. J., Ferguson A. M. N., Ibata R. A., Lewis G. F., Tanvir N., 2005, *MNRAS*, 356, 979
- McConnachie A. W., Irwin M. J., Lewis G. F., Ibata R. A., Chapman S. C., Ferguson A. M. N., Tanvir N. R., 2004, *MNRAS*, 351, L94
- Meléndez J., Asplund M., Alves-Brito A., Cunha K., Barbay B., Bessell M. S., Chiappini C., Freeman K. C., Ramírez I., Smith V. V., Yong D., 2008, *A&A*, 484, L21
- Merrett H. R., Merrifield M. R., Douglas N. G., Kuijken K., Romanowsky A. J., Napolitano N. R., Arnaboldi M., Capaccioli M., Freeman K. C., Gerhard O., Coccato L., Carter D., Evans N. W., Wilkinson M. I., Halliday C., Bridges T. J., 2006, *MNRAS*, 369, 120
- Park C., Choi Y., Vogeley M. S., Gott III J. R., Blanton M. R., 2007, *ApJ*, 658, 898
- Peñarrubia J., McConnachie A., Babul A., 2006, *ApJ*, 650, L33
- Pohlen M., Dettmar R., Lütticke R., 2000, *A&A*, 357, L1
- Purcell C. W., Bullock J. S., Kazantzidis S., 2010, *MNRAS*, 404, 1711
- Purcell C. W., Kazantzidis S., Bullock J. S., 2009, *ApJ*, 694, L98
- Quillen A. C., Minchev I., Bland-Hawthorn J., Haywood M., 2009, *MNRAS*, 397, 1599
- Quinn P. J., Hernquist L., Fullagar D. P., 1993, *ApJ*, 403, 74
- Read J. I., Lake G., Agertz O., Debattista V. P., 2008, *MNRAS*, 389, 1041
- Reddy B. E., Lambert D. L., Allende Prieto C., 2006, *MNRAS*, 367, 1329
- Richardson J. C., Ferguson A. M. N., Johnson R. A., Irwin M. J., Tanvir N. R., Faria D. C., Ibata R. A., Johnston

- K. V., Lewis G. F., McConnachie A. W., Chapman S. C., 2008, *AJ*, 135, 1998
- Robertson B., Bullock J. S., Cox T. J., Di Matteo T., Hernquist L., Springel V., Yoshida N., 2006, *ApJ*, 645, 986
- Robin A. C., Haywood M., Creze M., Ojha D. K., Bienayme O., 1996, *A&A*, 305, 125
- Robin A. C., Reylé C., Derrière S., Picaud S., 2004, *A&A*, 416, 157
- Roškar R., Debattista V. P., Brooks A. M., Quinn T. R., Brook C. B., Governato F., Dalcanton J. J., Wadsley J., 2010, *MNRAS*, 408, 783
- Roškar R., Debattista V. P., Quinn T. R., Stinson G. S., Wadsley J., 2008, *ApJ*, 684, L79
- Rutledge G. A., Hesser J. E., Stetson P. B., 1997, *PASP*, 109, 907
- Saglia R. P., Fabricius M., Bender R., Montalto M., Lee C., Riffeser A., Seitz S., Morganti L., Gerhard O., Hopp U., 2010, *A&A*, 509, A61+
- Sales L. V., Helmi A., Abadi M. G., Brook C. B., Gómez F. A., Roškar R., Debattista V. P., House E., Steinmetz M., Villalobos Á., 2009, *MNRAS*, 400, L61
- Schönrich R., Binney J., 2009a, *MNRAS*, 396, 203
- Schönrich R., Binney J., 2009b, *MNRAS*, 399, 1145
- Seigar M. S., Barth A. J., Bullock J. S., 2008, *MNRAS*, 389, 1911
- Sellwood J. A., Binney J. J., 2002, *MNRAS*, 336, 785
- Sellwood J. A., Nelson R. W., Tremaine S., 1998, *ApJ*, 506, 590
- Shaw M. A., Gilmore G., 1989, *MNRAS*, 237, 903
- Simon J. D., Geha M., 2007, *ApJ*, 670, 313
- Soubiran C., Bienaymé O., Siebert A., 2003, *A&A*, 398, 141
- Stewart K. R., Bullock J. S., Barton E. J., Wechsler R. H., 2009, *ApJ*, 702, 1005
- Stewart K. R., Bullock J. S., Wechsler R. H., Maller A. H., Zentner A. R., 2008, *ApJ*, 683, 597
- Toth G., Ostriker J. P., 1992, *ApJ*, 389, 5
- Tsikoudi V., 1979, *ApJ*, 234, 842
- van den Bergh S., 1999, *A&A Rev*, 9, 273
- van der Kruit P. C., 1984, *A&A*, 140, 470
- van der Kruit P. C., Searle L., 1981, *A&A*, 95, 105
- van Dokkum P. G., Peletier R. F., de Grijs R., Balcells M., 1994, *A&A*, 286, 415
- Velazquez H., White S. D. M., 1999, *MNRAS*, 304, 254
- Villalobos Á., Helmi A., 2009, *MNRAS*, 399, 166
- Villumsen J. V., 1985, *ApJ*, 290, 75
- Walker I. R., Mihos J. C., Hernquist L., 1996, *ApJ*, 460, 121
- Walterbos R. A. M., Braun R., 1994, *ApJ*, 431, 156
- Walterbos R. A. M., Kennicutt Jr. R. C., 1988, *A&A*, 198, 61
- Widrow L. M., Perrett K. M., Suyu S. H., 2003, *ApJ*, 588, 311
- Wyse R. F. G., Gilmore G., Norris J. E., Wilkinson M. I., Kleya J. T., Koch A., Evans N. W., Grebel E. K., 2006, *ApJ*, 639, L13
- Yin J., Hou J. L., Prantzos N., Boissier S., Chang R. X., Shen S. Y., Zhang B., 2009, *A&A*, 505, 497
- Yoachim P., Dalcanton J. J., 2006, *AJ*, 131, 226
- Yoachim P., Dalcanton J. J., 2008a, *ApJ*, 683, 707
- Yoachim P., Dalcanton J. J., 2008b, *ApJ*, 682, 1004